ADVANCES IN ATMOSPHERIC SCIENCES, VOL. 39, DECEMBER 2022, 2087–2106

• **Original Paper** •

Relationships between Cloud Droplet Spectral Relative Dispersion and Entrainment Rate and Their Impacting Factors※

Shi LUO[1,2], Chunsong LU[*2], Yangang LIU[3], Yaohui LI[1], Wenhua GAO[4], Yujun QIU[2], Xiaoqi XU[5], Junjun LI[2], Lei ZHU[2], Yuan WANG[6], Junjie WU[1], and Xinlin YANG[1]

[1]*College of Aviation Meteorology*, *Civil Aviation Flight University of China*, *Guanghan* 618307, *China*

[2]*Collaborative Innovation Center on Forecast and Evaluation of Meteorological Disasters (CIC-FEMD)/ Key Laboratory for Aerosol-Cloud-Precipitation of China Meteorological Administration*, *Nanjing University of Information Science & Technology*, *Nanjing* 210044, *China*

[3]*Environmental and Climate Sciences Department*, *Brookhaven National Laboratory*, *Upton*, *New York* 11973, *US*

[4]*State Key Laboratory of Severe Weather*, *Chinese Academy of Meteorological Sciences*, *Beijing* 100081, *China*

[5]*Nanjing Joint Institute for Atmospheric Sciences*, *Nanjing* 210019, *China*

[6]*Collaborative Innovation Center for Western Ecological Safety*, *Lanzhou University*, *Lanzhou* 730000, *China*

(Received 9 November 2021; revised 8 April 2022; accepted 6 May 2022)

ABSTRACT

Cloud microphysical properties are significantly affected by entrainment and mixing processes. However, it is unclear how the entrainment rate affects the relative dispersion of cloud droplet size distribution. Previously, the relationship between relative dispersion and entrainment rate was found to be positive or negative. To reconcile the contrasting relationships, the Explicit Mixing Parcel Model is used to determine the underlying mechanisms. When evaporation is dominated by small droplets, and the entrained environmental air is further saturated during mixing, the relationship is negative. However, when the evaporation of big droplets is dominant, the relationship is positive. Whether or not the cloud condensation nuclei are considered in the entrained environmental air is a key factor as condensation on the entrained condensation nuclei is the main source of small droplets. However, if cloud condensation nuclei are not entrained, the relationship is positive. If cloud condensation nuclei are entrained, the relationship is dependent on many other factors. High values of vertical velocity, relative humidity of environmental air, and liquid water content, and low values of droplet number concentration, are more likely to cause the negative relationship since new saturation is easier to achieve by evaporation of small droplets. Further, the signs of the relationship are not strongly affected by the turbulence dissipation rate, but the higher dissipation rate causes the positive relationship to be more significant for a larger entrainment rate. A conceptual model is proposed to reconcile the contrasting relationships. This work enhances the understanding of relative dispersion and lays a foundation for the quantification of entrainment-mixing mechanisms.

Key words: clouds, entrainment rate, relative dispersion of cloud droplet size distribution, mixing and evaporation

Citation: Luo, S., and Coauthors, 2022: Relationships between cloud droplet spectral relative dispersion and entrainment rate and their impacting factors. *Adv. Atmos. Sci.*, **39**(12), 2087−2106, https://doi.org/10.1007/s00376-022-1419-5.

Article Highlights:

- The observed contrasting relationships between the relative dispersion of cloud droplet size distribution and entrainment rate are reproduced, and their impacting factors are examined.
- The different relationships are mainly determined by the relative importance of evaporation of small and big droplets, and entrained cloud condensation nuclei.
- The negative relationship is more likely to occur for high values of vertical velocity, relative humidity of environmental air, and liquid water content, and low values of droplet number concentration.

1. Introduction

In the Earth system, clouds are key components that affect the radiation balance, hydrologic cycle, and weather/climate (Xue and Feingold, 2006; Li and Zhang, 2017; Zelinka

※ This paper is a contribution to the special issue on Cloud–Aerosol–Radiation–Precipitation Interaction: Progress and Challenges

* Corresponding author: Chunsong LU
Email: luchunsong110@gmail.com

et al., 2017; Randall et al., 2018; Zhao et al., 2018; Liu, 2019; Wang et al., 2019, 2020b, 2020c, 2021b; Xu et al., 2020; Zheng et al., 2021). The spectral broadening of cloud droplet size distribution (CDSD) is a long-standing problem in the cloud physics community (Devenish et al., 2012; Cooper et al., 2013; Lu et al., 2018a). The classical theoretical condensation equation (Wallace and Hobbs, 2006) predicts a narrow CDSD since the growth rate of a cloud droplet radius is inversely proportional to the radius. In nature, the observed CDSD is usually wider than that from the theoretical expectation (Johnson, 1993). The cloud physics community has not yet fully understood the mechanisms contributing to the broadening (Devenish et al., 2012; Cooper et al., 2013; Lu et al., 2018a). The spectral width is well known to have significant impacts on the collision-coalescence between cloud droplets (Yum and Hudson, 2005; Cooper et al., 2013), cloud radiative properties (Liu et al., 2002), cloud water sedimentation flux (Ackerman et al., 2009), precipitation formation (Xie et al., 2013), and cloud-climate feedbacks (Liu et al., 2002; Zhao et al., 2006; Tas et al., 2012, 2015; Liu, 2019). The spectral width is usually expressed by the standard deviation of cloud droplet size or the relative dispersion (d, the ratio of standard deviation to mean radius) (Liu and Daum, 2002; Rotstayn and Liu, 2009; Pandithurai et al., 2012; Tas et al., 2015; Prabhakaran et al., 2020; Wang et al., 2020a, 2021a; Bera, 2021). Various factors are reported to affect d, including supersaturation fluctuation (Chandrakar et al., 2016), vertical velocity (Liu et al., 2006; Hudson et al., 2012; Chen et al., 2016), aerosol loading (Peng et al., 2007; Chandrakar et al., 2016; Chen et al., 2016), and entrainment-mixing processes (Lu et al., 2013a; Luo et al., 2020, 2021; Wang et al., 2020b). However, to date the factors affecting d, particularly the contribution of the entrainment-mixing processes, have not been completely understood by the physics community.

Entrainment-mixing processes affect the spectral shape of CDSD by altering the droplets' trajectories and the local environment of the droplets (Cooper, 1989; Krueger et al., 1997; Lasher-Trapp et al., 2005; Kumar et al., 2012). Based on simulations and observations, d is larger in diluted clouds than other clouds (i.e., d increases during the entrainment-mixing processes) (Lasher-Trapp et al., 2005; Prabha et al., 2012; Bera et al., 2016a, b). Recently, Bera (2021) reported that d increases as dilution increases, and reactivation and incomplete evaporation are responsible for the slight broadening of small droplets in the low dilution regime.

Despite several efforts, the quantitative effects of the entrainment and mixing process on microphysical properties remain elusive. In particular, the relationship between d and fractional entrainment rate (λ) has been rarely studied. The entrainment rate describes how fast environmental air is entrained into clouds and subsequently mixes with the in-cloud air. The value of λ is defined as the ratio of the entrained mass of environmental air into the cloud to the cloud mass itself per unit height and is essential to the parameterization of cumulus clouds (Turner, 1962; Raga et al., 1990; Houze, 1993; Lu et al., 2012; de Rooy et al., 2013; Zhang et al., 2016; Lu et al., 2018c; Stanfield et al., 2019; Xu et al., 2021; Zhu et al., 2021). The observational results of Lu et al. (2013a) revealed that d increases with increasing λ, owing to a nearly constant standard deviation and reduced mean radius with increasing λ. However, Guo et al. (2018) reported that d is negatively correlated with λ because small droplets evaporate more quickly than big droplets. Overall, these contrasting relationships need to be reconciled.

To address this issue, the positive/negative correlations between d and λ are reproduced with the Explicit Mixing Parcel Model (EMPM) in this study. The role of entrained cloud condensation nuclei (CCN) is emphasized to determine the relationship between the two quantities. The sources of small droplets are tracked, and the influencing factors, including vertical velocity, relative humidity of entrained environmental air, turbulence dissipation rate, droplet number concentration, and liquid water content, are analyzed. Finally, a conceptual model is established based on the results.

In the rest of the paper, section 2 describes the EMPM model and methods. Section 3 presents the relationship between d and λ with and without entrained CCN. The effects of key factors influencing the relationship are determined. The conclusions are given in section 4.

2. Model and Methods

2.1. *Model Description*

The EMPM model developed by Kerstein (1992), Krueger et al. (1997), Su et al. (1998), Krueger et al. (2008), and Tölle and Krueger (2014) has been extensively utilized to study the entrainment-mixing processes between cloud and the ambient air (e.g., Krueger et al., 1997, 2008; Su et al., 1998; Lu et al., 2013b, 2018b, 2020; Tölle and Krueger, 2014; Luo et al., 2020, 2021). The EMPM can track the history of every droplet due to the variation of the local environment, ranging from the model integral scale to the model Kolmogorov scale (~1 mm). During the entrainment-mixing process, four processes are considered: parcel ascent, entrainment, turbulent mixing (i.e., turbulent deformation and molecular diffusion), and droplet condensation/evaporation. Turbulent deformation is a key process and is implemented by random rearrangement events as a finite-rate turbulent mixing. Using the "triplet map" introduced by Kerstein (1991), each event can be realized. The "triplet map" replaces the scalar field within the randomly selected segment with three compressed copies of the scalar field and then inverts the central copy (Krueger et al., 1997; Su et al., 1998). This treatment changes the scalar gradient within the segment and realizes the effect of compressive strain in a turbulent flow (Krueger et al., 1997; Su et al., 1998). The finite-rate mixing has been supported by observations (Gerber et al., 2008) and is beneficial to the broadening of CDSD. This setting allows individual droplet to experience different local supersaturation environment and contribute to the different condensation/evaporation

rate (Su et al., 1998).

When entrainment occurs, a randomly selected region of the parcel is replaced with environmental air. The subsequent turbulent mixing process includes two stages. In the first stage, the entrained air breaks down under the action of turbulent eddies and randomly distributes within the cloudy parcel. This stage increases the interfacial area between the cloudy air and entrained air. In the second stage, when entrained air size approaches the Kolmogorov microscale, the molecular diffusion process takes effect and rapidly smooths out the scalar gradients (Krueger et al., 1997; Su et al., 1998; Tölle and Krueger, 2014). A more detailed description of the EMPM has been provided by Krueger et al. (1997), Su et al. (1998), Krueger et al. (2008), and Tölle and Krueger (2014). The length, width, and height of the EMPM domain are 20 m, 1 mm, and 1 mm, respectively. Su et al. (1998) tested the sensitivity to sizes equaling 100 m and 20 m. The simulations indicated that "the 100-m results are similar to those from the 20-m case ". Further, the EMPM works as follows: the entire EMPM domain containing droplets is treated as a cloudy parcel and ascends at a specific vertical velocity across the entire domain. When the entrainment-mixing process occurs, environmental air replaces the same-sized cloudy parcel at the entrainment height. During the subsequent ascending process, the entrained environmental air mixes with the cloudy air at a finite turbulent rate ("Mix 1 "). Subsequently, the cloud grows adiabatically ("Adiabatic") until another entrainment-mixing process occurs ("Mix 2"). Notably, the cloud continues to ascend during the three stages.

The initial droplets in the cloudy parcel are assumed to follow a gamma size distribution (Liu et al., 2002; McFarquhar et al., 2015; Lu et al., 2020; Bera, 2021), such that the droplet number concentration $n(r)$ for a droplet radius (r) is given as:

$$n(r) = N_0 r^{\mu} e^{-\beta r}, \quad (1)$$

where N_0, β, and μ represent the intercept, slope, and shape parameters, respectively. The narrow initial CDSD has μ and d of 40.0 and 0.16, respectively, and is binned by 49 bins, ranging from 1 to 25 μm in radius (Fig. S1 in the Electronic Supplementary Material, ESM). During ascent, the first entrainment-mixing process is set to occur near the beginning of the simulations to examine the effects of entrainment-mixing on the narrow CDSD. Since the model output frequency is 0.75 s, the first entrainment process is chosen to occur at 0.75 s. During the subsequent adiabatic process, d first increases and then decreases. The formation of small droplets increases d and the growth of small droplets into big droplets by condensation decreases d, as per the theoretical expectation of droplet growth (Wallace and Hobbs, 2006). The second entrainment-mixing process occurs when d reaches its maximum. Such a choice is employed to weaken the significant effect of the condensation process, which results in a decrease in d. Herein, we mainly focus on the relationship between d and λ after the second entrainment-mixing process.

The cloudy parcel has initial pressure, water vapor mixing ratio, and temperature of 963.95 hPa, 15.73 g kg^{-1}, and 293.56 K (Raga et al., 1990; Tölle and Krueger, 2014), respectively. The baseline case of the EMPM has a vertical velocity (w) of 1.0 m s^{-1}, relative humidity of entrained environmental air (RH_e) of 88%, turbulence dissipation rate (ε) of 5×10^{-3} m^2 s^{-3}, initial droplet number concentration (n_i) of 119.4 cm^{-3}, initial liquid water content (LWC_i) of 0.5 g m^{-3}, and initial mean volume radius (r_{vi}) of 10 μm. Further, entrained environmental air is assumed to be without and with CCN (Cases without and with CCN are considered.). According to Su et al. (1998) and Krueger et al. (2008), the CCN distribution is composed of two log-normal size distributions. The first one is 18 categories of salt with the radius range of 0.14–3.73 μm; the mean and standard deviation are 0.9 μm and 0.63 μm, respectively. The second one is 31 categories of ammonia bi-sulfate with the radius range of 0.02–0.75 μm; the mean and standard deviation are 0.09 μm and 0.05 μm, respectively; the CCN concentration is 49.65 cm^{-3}. These CCN are assumed to be at equilibrium sizes, and the competition for water vapor between CCN and droplets is considered. The growth of each droplet is dependent on its local meteorological fields, and the curvature and solution effects of droplet are considered (see Appendix for the droplet growth equations).

Previous measurements and numerical simulations in shallow cumulus clouds indicate that ε can range from 10^{-5} to 10^{-2} m^2 s^{-3} (Siebert et al., 2006a, b; Hoffmann et al., 2014); w can increase from near 0 at cloud edge to 6 m s^{-1} in the core of the convective cloud (Jonas, 1990; Burnet and Brenguier, 2007; Hudson et al., 2012); LWC is between 0.1 g m^{-3} and 1.2 g m^{-3} (Gerber et al., 2008; Hudson et al., 2012); n_i can vary from 20 to 700 cm^{-3} (Burnet and Brenguier, 2007; Gerber et al., 2008; Small and Chuang, 2008; Hudson et al., 2012); and RH_e can be in the range of 70% –95% (Axelsen, 2005; Burnet and Brenguier, 2007; Lu et al., 2018c). To explore the effects of impact factors on the relationship between d and λ, the w values in the domain are set to 0.5, 1.0, and 1.5 m s^{-1}, respectively; the RH_e values are set to 77%, 88%, and 93.5%, respectively; the ε values are set to 5×10^{-4}, 5×10^{-3}, and 1×10^{-2} m^2 s^{-3}, respectively; the n_i values are set to 69.1, 119.4, and 552.6 cm^{-3}, computed from LWC_i of 0.5 g m^{-3} and r_{vi} of 12, 10, and 6 μm, respectively. LWC_i of 0.25, 0.5, and 0.75 g m^{-3} are also included with a fixed r_{vi} of 10 μm. The above parameter settings are listed in Table 1. These values in the sensitivity tests are within reasonable ranges and represent typical shallow convective clouds with distinct environmental thermodynamics and air pollution amounts.

2.2. *Methods*

As mentioned above, we concentrate on the second entrainment-mixing process and further investigate the relationship between d and λ. Here, λ is calculated using the method developed by Lu et al. (2012):

Table 1. Parameters of sensitivity simulations.

Cases	Entrained Cloud Condensation Nuclei, CCN	Vertical velocity, w (m s^{-1})	Relative humidity of entrained air, RH$_e$ (%)	Turbulence dissipation rate, ε (m^2 s^{-3})	Initial droplet number concentration, n_i (cm^{-3})	Initial liquid water content, LWC$_i$ (g m^{-3})	Entrained air blob number of the second entrainment-mixing process (N_2)
Baseline case	Yes	1.0	88	5×10^{-3}	119.4	0.5	2, 4, 6, 8, 10
Case 1: Entrained CCN effect	No	1.0	88	5×10^{-3}	119.4	0.5	2, 4, 6, 8, 10
Case 2: w effect	Yes	0.5, 1.0, 1.5	88	5×10^{-3}	119.4	0.5	2, 4, 6, 8, 10
Case 3: RH$_e$ effect	Yes	1.0	77, 88, 93.5	5×10^{-3}	119.4	0.5	2, 4, 6, 8, 10
Case 4: ε effect	Yes	1.0	88	5×10^{-4}, 5×10^{-3}, 1×10^{-2}	119.4	0.5	2, 4, 6, 8, 10
Case 5: n_i effect	Yes	1.0	88	5×10^{-3}	69.1, 119.4, 552.6	0.5	2, 4, 6, 8, 10
Case 6: LWC$_i$ effect	Yes	1.0	88	5×10^{-3}	119.4	0.25, 0.5, 0.75	2, 4, 6, 8, 10

$$\lambda = -\frac{\ln(\chi)}{h}, \tag{2a}$$

$$\chi = \chi_1^* \chi_2^*, \tag{2b}$$

$$\chi_1^* = 1 - \frac{N_1 l}{L}, \tag{2c}$$

$$\chi_2^* = 1 - \frac{N_2 l}{L}. \tag{2d}$$

where L is the length of EMPM; χ is the integrated fraction of the adiabatic cloud; χ_1^* and χ_2^* are the fractions of the adiabatic cloud at the first and second entrainment heights, respectively; and N_1 and N_2 are the entrained environmental air blob numbers for the first and second entrainment-mixing processes, respectively. Evidently, λ is determined by N_2, given each entrained environmental air blob size (l) of 0.5 m, N_1 of 10, and the entrainment height above cloud base (h). The baseline case is taken as an example to calculate λ. The corresponding height of the initial CDSD is 204.5 m above the cloud base and is calculated by assuming that the cloud parcel with LWC$_i$ = 0.5 g m^{-3} moves downward until LWC$_i$ = 0 g m^{-3}. As the second entrainment occurs at 42.75 s and w is 1 m s^{-1}, h is equal to 42.75 m + 204.5 m (i.e., 247.25 m). As expected, a larger N_2 corresponds to a larger λ (Fig. S2 in the ESM), and λ exists in a reasonable range, from 1.35 to 2.29 km^{-1} (Lu et al., 2012; de Rooy et al., 2013). N_2 is used hereafter to refer to λ. For cases with and without entrained CCN, the relationship between d and λ is investigated by setting different N_2 values. In the cases of baseline and all sensitivity simulations, N_2 are set to 2, 4, 6, 8, and 10, respectively, with a fixed N_1 of 10. Different N_1 values (2, 4, 6, 8, 10) are also tested, and as expected, a larger N_1 leads to a larger d after the first entrainment-mixing process (Fig. S3 in the ESM); this is because the initial adiabatic CDSD is narrow (Tölle and Krueger, 2014; Gao et al., 2018; Luo et al., 2020). Therefore, d and λ are positively correlated. Since this relationship between d and λ is well known for adiabatic narrow CDSD, we focus on the second entrainment-mixing process and select the widest CDSD at the beginning of the second entrainment-mixing process (i.e., at the end of the first entrainment-mixing process). The CDSD after the first entrainment-mixing process for N_1 = 10 is the widest and has the biggest difference from the adiabatic CDSD. Therefore, N_1 is set to 10.

3. Results

3.1. *Reproduction of the Positive/Negative Correlation between Relative Dispersion and Entrainment Rate*

As mentioned above, different N_2 values are employed in the EMPM model to determine the relationship between d and λ. As previous studies revealed that entrained CCN has a significant impact on microphysical properties (Lasher-trapp et al., 2005; Gerber et al., 2008; Krueger et al., 2008; Slawinska et al., 2012; Hoffmann et al., 2015; Bera et al., 2016b; Yeom et al., 2019; Chen et al., 2020), it should be interesting to explore if and how entrained CCN affect the reproduction of positive and negative correlations between d and λ. The d value occurring when new saturation is achieved after the second entrainment-mixing process is the one employed to assess the relationship between d and λ. For the criterion of new saturation, the domain-averaged supersaturation should be greater than 99.5% (Lehmann et al., 2009; Luo et al., 2020).

3.1.1. *Positive Correlation*

Two experiments are conducted (one with entrained CCN and the other without). In the group of entrained CCN, entrained air contains CCN during both the first and second entrainment-mixing processes. In the other group, entrained CCN is not considered during the two entrainment-mixing processes. Figures 1a, 1c, 1e, and 1g show the temporal evolutions of d, droplet number concentration (n_c), liquid water content (LWC_c), and mean radius (r_m), respectively, in the simulation without entrained CCN (i.e., Case 1 in Table 1). The increase in d is accompanied by the notable decreases in LWC_c and r_m (Figs. 1a, 1e, 1g) during the first entrainment-mixing process (before the triangle, determined by the criterion of the domain-averaged supersaturation greater than 99.5%). The broadening of CDSD is attributed to the partial evaporation of big droplets (Figs. S4, S5 in the ESM) (e.g., Yum and Hudson, 2005; Lu et al., 2013a; Kumar et al., 2014; Tölle and Krueger, 2014; Gao et al., 2018; Luo et al., 2020). Further, only a slight decrease in n_c is observed (Fig. 1c) during mixing, suggesting a homogeneous mixing type, as droplet size decreases whereas number concentration remains virtually unchanged during homogeneous mixing (Baker et al., 1980; Lu et al., 2013b; Tölle and Krueger, 2014).

During the adiabatic process (between the triangle and pentagram in Fig. 1), the reactivation of deactivated CCN from complete evaporation of droplets occurs due to supersaturation (Yang et al., 2018; Bera, 2021). However, the amount of reactivation of deactivated CCN is small; only a small peak of droplets near 1.0 μm in radius is observed (Figs. S4, S5). A radius of 1.0 μm is employed as the criterion that separates cloud droplets from aerosols (Hsieh et al., 2009; Ma et al., 2010; Small et al., 2013; Yum et al., 2015; Bera et al., 2016a; Lu et al., 2020). Therefore, d and n_c vary slightly, and r_m increases due to the condensation process (Figs. 1a, 1c, 1g). During the second entrainment-mixing process (after the pentagram in Fig. 1a), n_c, LWC_c, and r_m decrease; d increases as N_2 increases. The broadening of CDSD towards small droplets by the evaporation of big droplets is more significant as N_2 increases (Figs. S4, S5). At the final states of the entrainment-mixing process, a larger N_2 has a larger d, suggesting a positive correlation between d and λ. This relationship aligns with that presented by Lu et al. (2013a) and conforms with commonly reported results that more entrained environmental air causes a more significant broadening of CDSD (Lasher-Trapp et al., 2005; Tölle and Krueger, 2014; Kumar et al., 2017).

3.1.2. *Negative Correlation*

Entrained CCN are also considered (i.e., the baseline case in Table 1), to further explore the relationship between d and λ. Of note, the microphysical properties display slight differences during the first entrainment-mixing process, compared with Case 1 without entrained CCN (Fig. 1). During the adiabatic process after the first entrainment-mixing process, water vapor condenses onto the entrained CCN, contributing to the formation of droplets (particles with a radius greater than 1.0 μm). These newly formed droplets significantly broaden CDSD and a remarkable peak of small droplets is observed (Figs. S4, S5), causing an increase in d and n_c and a decrease in r_m (Figs. 1b, 1d,1h). This pronounced increase in d aligns with the statements made by Telford and Chai (1980), Lasher-Trapp et al. (2005), Krueger et al. (2008), and Yeom et al. (2019). For instance, Yeom et al. (2019) reported that a higher droplet number concentration corresponds to a higher d due to the secondary activation of aerosol. As expected, n_c in the baseline case is greater than that without entrained CCN (Figs. 1c, 1d), and LWC_c is comparable in the two cases (Figs. 1e, 1f). In contrast, r_m is smaller when entrained CCN is considered (Figs. 1g, 1h). During the second entrainment-mixing process, d monotonically decreases, and r_m increases due to the substantial evaporation of small droplets with mixing time for $N_2 \leqslant 8$. The peak of small droplets in CDSD gradually decreases (Figs. S4, S5). However, when $N_2 = 10$, d first decreases and then increases; correspondingly, r_m first increases and then decreases, which is discussed in detail later. When new saturation is achieved after the second entrainment-mixing process, a larger N_2 has a smaller d when N_2 increases from 2 to 8 (Fig. 1b), suggesting a negative correlation between d and λ. Such a finding is supported by Guo et al. (2018) who found that d decreased as λ increased. However, when N_2 increases from 8 to 10, d and λ are found to be positively correlated.

The effects of entrained l are examined by setting $l = 1$ m and $N_2 = 1, 2, 3, 4, 5$ to keep the fraction of entrained environmental air the same as that in the baseline case. As shown in Fig. S6, the blob size may affect the detailed response of cloud microphysics to entrained air but does not affect the main conclusions.

3.1.3. *Physical Mechanisms*

Guo et al. (2018) highlighted the role of small droplets in determining the negative relationship between d and λ. Tölle and Krueger (2014) and Luo et al. (2020) also revealed the effects of small droplets on d. Here, small droplets are separated by the criterion of radius less than 3.0 μm. The ratio of small droplet number concentration (n_s) to total droplet number concentration (n_c) in Fig. 2a is similar to that of d in Fig. 1a without entrained CCN, suggesting that n_s is a key property in determining d. The evolution of the two properties with entrained CCN also support this argument. Altogether, these results confirm the positive correlation between n_s and d reported by Luo et al. (2020).

To clearly explain the physical mechanisms in the above negative and positive correlations between d and λ, small droplets are tracked with the EMPM model, which can track the history of each droplet. Figure 2 shows the sources of small droplets and the proportions of small and big droplets (radius greater than 3.0 μm). Two sources of small droplets are included: partial evaporation of big droplets during mixing and evaporation, and condensation on the entrained CCN, which is consistent with the observa-

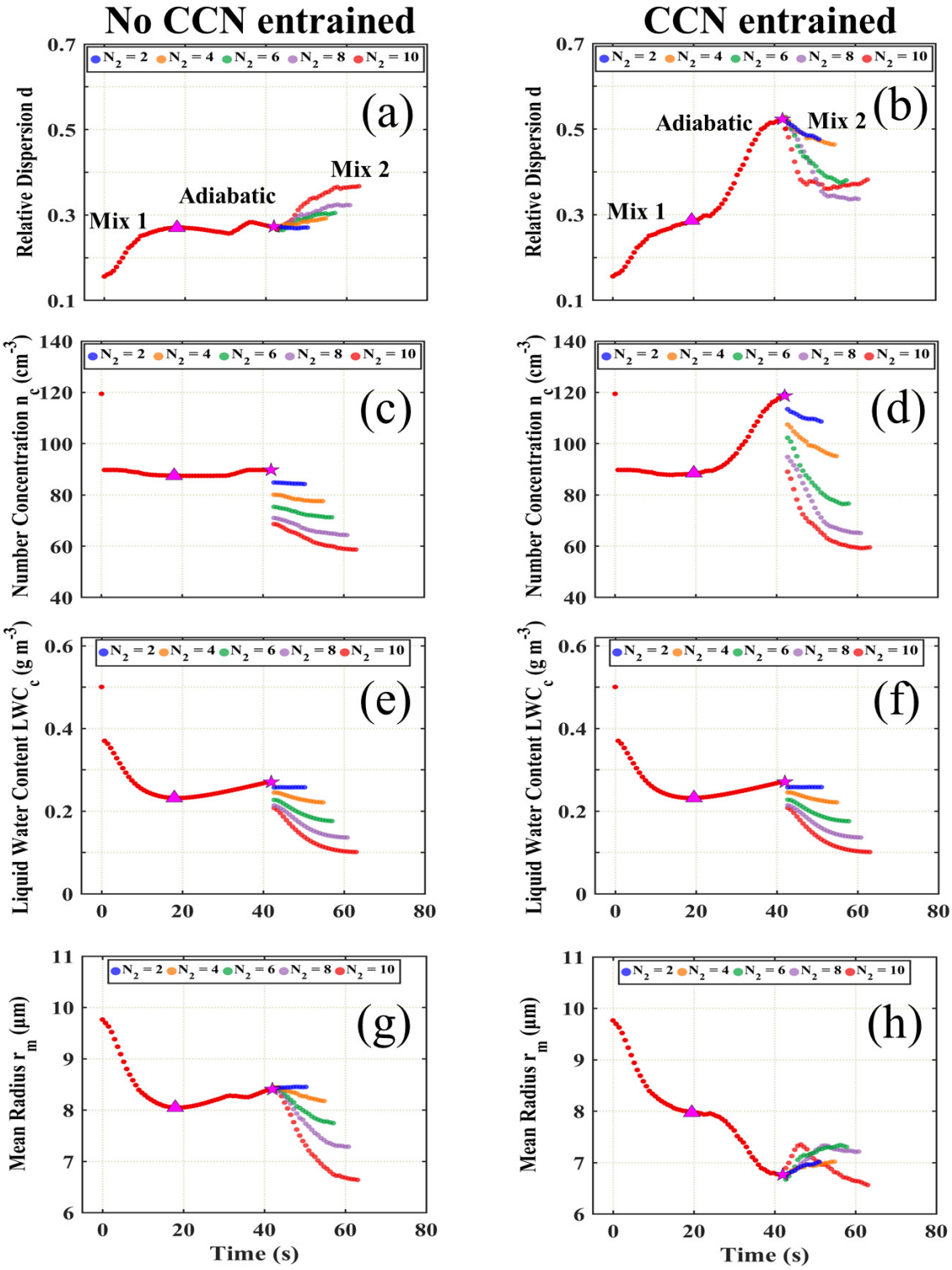

Fig. 1. Temporal evolutions of cloud droplet spectral relative dispersion (d), droplet number concentration (n_c), liquid water content (LWC_c), and mean radius (r_m) with the entrained environmental air blob number of the second entrainment-mixing process (N_2) equal to 2, 4, 6, 8, and 10. Left: entrained environmental air without cloud condensation nuclei (CCN). Right: entrained environmental air with CCN. The triangle and pentagram represent the ending of the first entrainment-mixing process ("Mix 1 ") and the beginning of the second entrainment-mixing process ("Mix 2"), respectively, as well as the adiabatic ascending process ("Adiabatic").

tion results of Bera (2021). Of note, the reactivation of deactivated CCN is negligible as discussed. As a result, this source is not included.

In Case 1 without entrained CCN, n_s/n_c increases as N_2

increases, which corresponds to the positive correlation between d and λ (Fig. 2a). Almost all small droplets arise from the partial evaporation of big droplets (Fig. 2e), though the accumulation of small droplets at the beginning of the second entrainment-mixing process is weak, with n_s/n_c of only ~ 6% (the pentagram in Fig. 2a). The small droplets evaporate faster and are easier to completely evaporate, compared with big droplets, mainly because of the relationship of $dr/dt \sim S/r$, where S is supersaturation and t is time (Wallace and Hobbs, 2006; Guo et al., 2018; Bera, 2021); the smaller the droplet size, the faster it evaporates. However, evaporation of these small droplets is not enough to saturate the entrained environmental air during the second entrainment-mixing process; to achieve new saturation, evaporation of big droplets is needed. Therefore, big droplets, instead of small droplets, dominate the evaporation process,

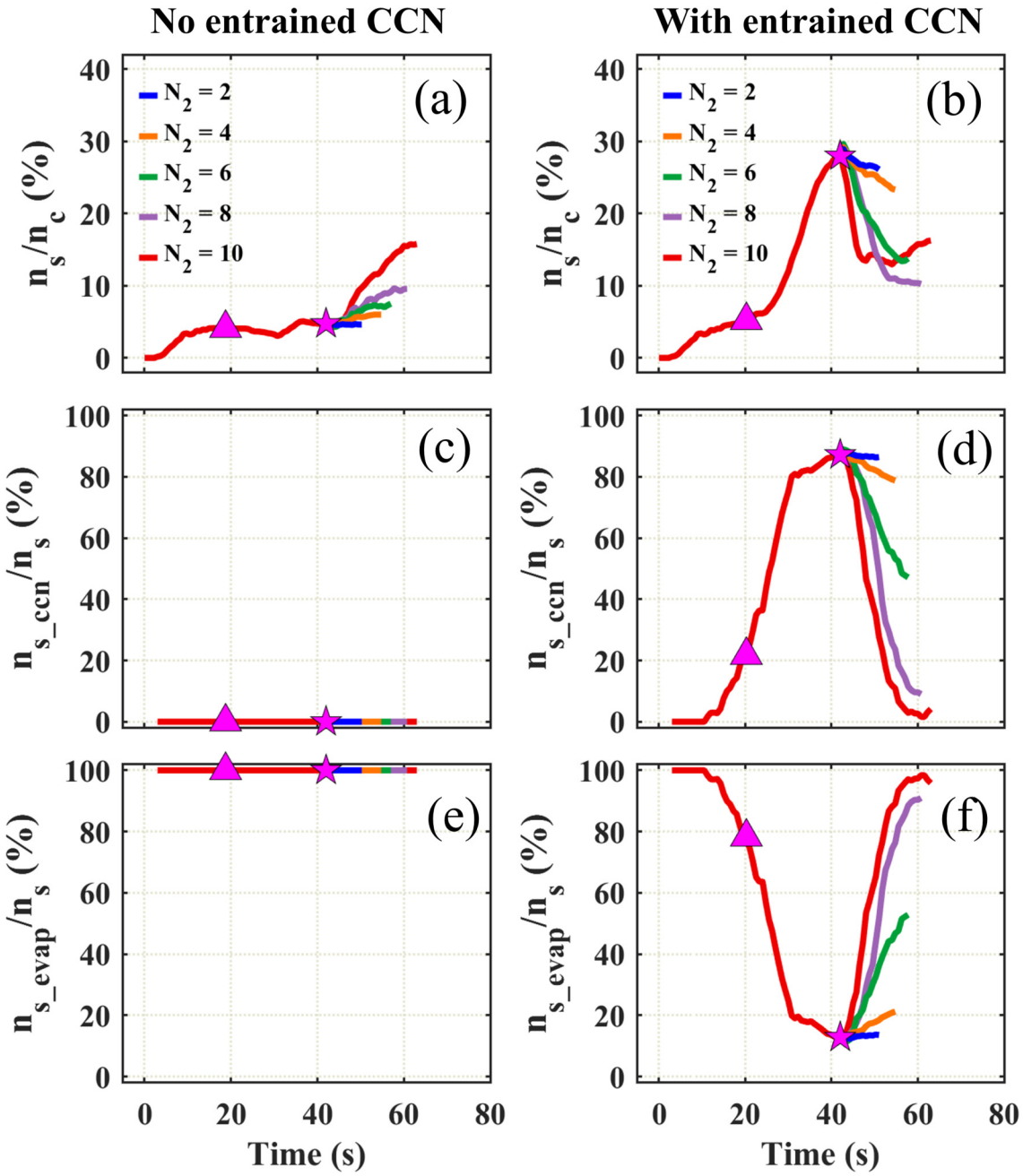

Fig. 2. Temporal evolutions of the ratios of (a, b) small droplet number concentration (n_s) to total droplet number concentration (n_c), (c, d) number concentration of small droplets originated from entrained cloud condensation nuclei (n_{s_ccn}) to n_s, and (e, f) number concentration of small droplets originated from big droplets evaporation (n_{s_evap}) to n_s, for the entrained environmental air blob numbers of the second entrainment-mixing process (N_2) equal to 2, 4, 6, 8, and 10. Left: environmental air without entrained cloud condensation nuclei (CCN). Right: environmental air with entrained CCN. The triangle and pentagram represent the ending of the first entrainment-mixing process and the beginning of the second entrainment-mixing process, respectively.

resulting in a positive correlation between d and λ.

In contrast to Case 1, small droplets account for 28% of total droplets at the beginning of the second entrainment-mixing process in the baseline case with entrained CCN (Fig. 2b). Almost 85% of small droplets are derived from the entrained CCN (Fig. 2d), whereas the remaining 15% are derived from the partial evaporation of big droplets (Fig. 2f). Figure 2b shows that n_s/n_c monotonically decreases with mixing time for $N_2 \leqslant 8$ during the second entrainment-mixing process, which is mainly attributed to the decrease in newly formed small droplets from the entrained CCN (Fig. 2d). As the entrained air is saturated due to evaporation being dominated by small droplets, d and λ are negatively correlated. It is challenging to determine the homogeneity of entrainment-mixing mechanisms (Gao et al., 2020, 2021). Theoretically, for homogeneous mixing, all droplets are exposed to the same subsaturated conditions and evaporate simultaneously (Lehmann et al., 2009; Lu et al., 2013b). Inhomogeneous mixing refers to the situation where only part of the cloudy air is affected by the mixing and therefore complete evaporation of all droplets in a small region of the cloud causes a significant decrease in number concentration (Baker et al., 1980). However, the decrease in number concentration is not necessarily caused by inhomogeneous mixing, but can also be a result of homogeneous mixing where all droplets experience the same subsaturated environment; in this case, small droplets in the entire cloudy air completely evaporate with the large droplets remaining in the cloudy air (Pinsky et al., 2016; Khain et al., 2018; Pinsky and Khain, 2018; Luo et al., 2021). When N_2 further increases to 10, the newly formed droplets from the entrained CCN decrease to nearly 0 (Fig. 2d). Since the new saturation of environmental air cannot be restored dominantly with the evaporation of these newly formed small droplets, the evaporation of big droplets dominates the process (Figs. S4, S5). As a result, the small droplets caused by the partial evaporation of big droplets increase (Fig. 2f). Combined with the two sources, n_s/n_c first decreases and then increases (Fig. 2b), and correspondingly, d first decreases and then increases for $N_2 = 10$ (Fig. 1b). The relationship between d and λ becomes positive when N_2 increases from 8 to 10, and $N_2 = 8$ is the transition point. Therefore, the relative evaporation significance of small droplets *vs*. big droplets determines n_s/n_c followed by the relationship between d and λ.

3.2. *Tests for the Sensitivity to Other Impacting Factors*

To further explore other impacting factors on the contrasting relationship between d and λ, sensitivity simulations are conducted according to the baseline case (with entrained CCN), as mentioned above. Table 1 lists all the sensitivity tests performed for different factors, including w, RH_e, ε, n_i, LWC_i, as these impacting factors are reported to significantly affect d (Peng et al., 2007; Hudson et al., 2012; Lu et al., 2013a; Chandrakar et al., 2016; Gao et al., 2018;Luo et al., 2020).

3.2.1. *Vertical Velocity*

The effects of w are determined when w values are set to 0.5, 1.0 (baseline), and 1.5 m s^{-1}, respectively (Case 2 in Table 1). Since the corresponding height of the initial CDSD is 204.5 m above cloud base at 0 s and the first entrainment process occurs at 0.75 s, the first entrainment heights of the three cases are 204.85 m, 205.25 m, and 205.63 m, respectively. Figure 3 shows the temporal evolutions of d. When $w = 0.5$ m s^{-1}, d and λ are negatively correlated for $N_2 \leqslant 6$, and positively correlated for $N_2 \geqslant 6$ (Fig. 3a). As a result, the N_2 value for the separation between the negative and positive correlations is 6 for $w = 0.5$ m s^{-1}. Further, this critical N_2 value is 8 for $w = 1.0$ m s^{-1} (Fig. 3b) and 10 for $w = 1.5$ m s^{-1} (Fig. 3c). Larger w conditions have more N_2 cases favoring the negative correlation between d and λ.

Figure 4 demonstrates that n_s/n_c (~ 19%) for $w = 0.5$ m s^{-1} is significantly smaller than that for $w = 1.5$ m s^{-1} (~ 30%) when the peak of d is obtained at the beginning of the second entrainment-mixing process (Figs. 4a, 4b). The droplet growth theory indicates that droplet growth rate is proportional to supersaturation, and larger w yields higher supersaturation (Wallace and Hobbs, 2006). As a result, the growth of entrained CCN into cloud droplets is more favorable with a stronger updraft. During the subsequent second entrainment-mixing process, n_s/n_c decreases for $N_2 \leqslant 6$ when $w = 0.5$ m s^{-1} (Fig. 4a) as the evaporation of a portion of these small droplets is sufficient to saturate the entrained environmental air. Such a finding corresponds with the negative correlation between d and λ. However, n_s/n_c first decreases and then increases for $N_2 \geqslant 8$ (Fig. 4a) due to the insufficient supply of small droplets to saturate the entrained environmental air. Evaporation of big droplets dominates the entrainment-mixing process for $N_2 \geqslant 8$ and n_s/n_c is subsequently increased (Fig. 4a). As a result, d and λ are positively correlated. In contrast, when $w = 1.5$ m s^{-1}, n_s/n_c decreases (Fig. 4b) with the dominant evaporation of small droplets, similar to the simulation with $w = 0.5$ m s^{-1} for $N_2 \leqslant 6$. Overall, larger w causes larger supersaturation and larger n_s from the entrained CCN; evaporation of small droplets is more likely to dominate during entrainment-mixing, and d and λ are more likely to be negatively correlated.

3.2.2. *Relative Humidity of the Entrained Environmental Air*

The effects of RH_e are determined with the same d values before the second entrainment-mixing process. Figure 5 shows the temporal evolutions of d for RH_e ranging from 77% to 93.5% (Case 3 in Table 1). When $RH_e = 93.5\%$ (Fig. 5c), d and λ are negatively correlated for $N_2 \leqslant 10$. However, only the first 4 and 3 N_2 cases favor the negative correlation between d and λ when $RH_e = 88\%$ and 77%, respectively (Figs. 5b, 5a). As a result, as RH_e increases, N_2 cases that favor the negative correlation between d and λ increase.

The behaviors of small droplets differ for $RH_e = 77\%$ and 93.5% (Fig. 6). When $RH_e = 77\%$, greater droplet evaporation is needed to restore the new saturation of entrained environmental air compared with that of $RH_e = 93.5\%$ (Tölle and Krueger, 2014; Pinsky and Khain, 2018; Luo et al., 2020). As a result, n_s/n_c first decreases and then

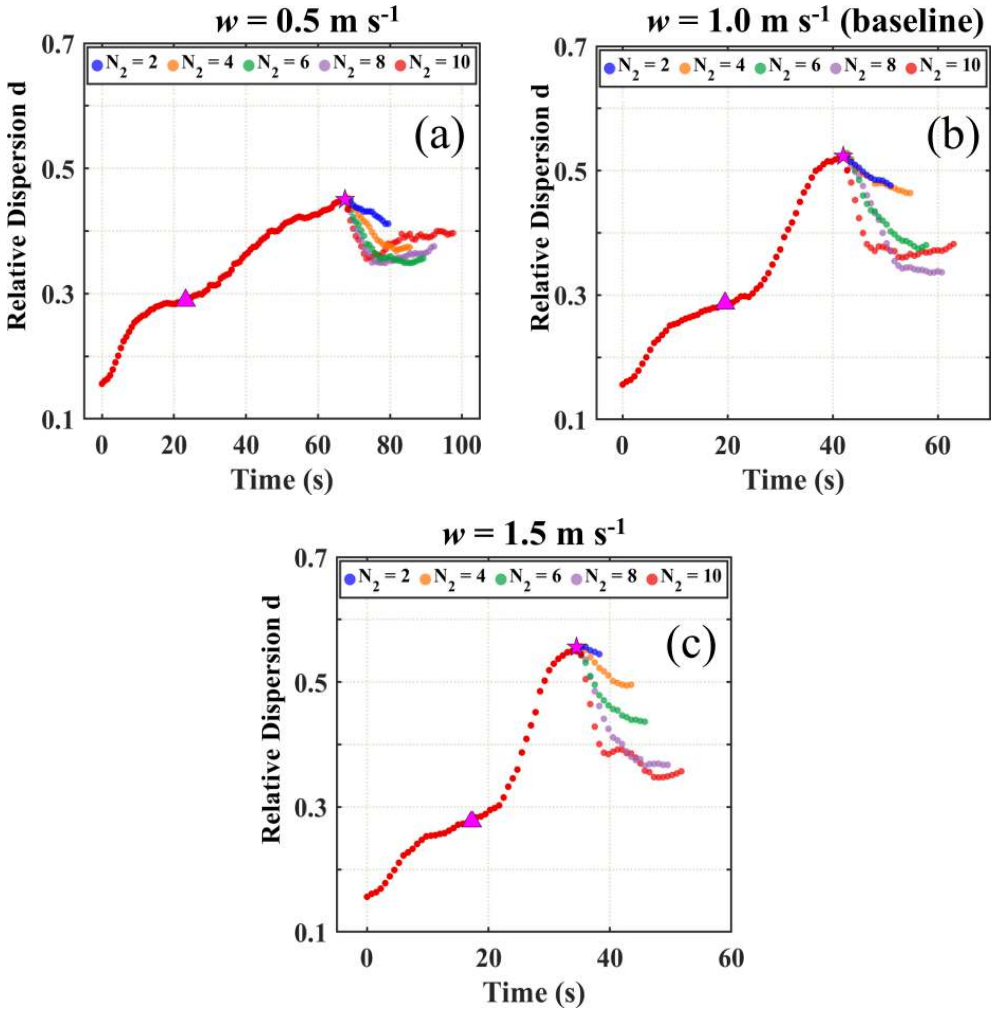

Fig. 3. Effects of vertical velocity (w) (Case 2 in Table 1). Temporal evolutions of relative dispersion for (a) w = 0.5 m s^{-1}, (b) w = 1.0 m s^{-1} (baseline case), and (c) w = 1.5 m s^{-1}. The entrained environmental air blob numbers of the second entrainment-mixing process (N_2) equal 2, 4, 6, 8, and 10. The triangle and pentagram represent the ending of the first entrainment-mixing process and the beginning of the second entrainment-mixing process, respectively.

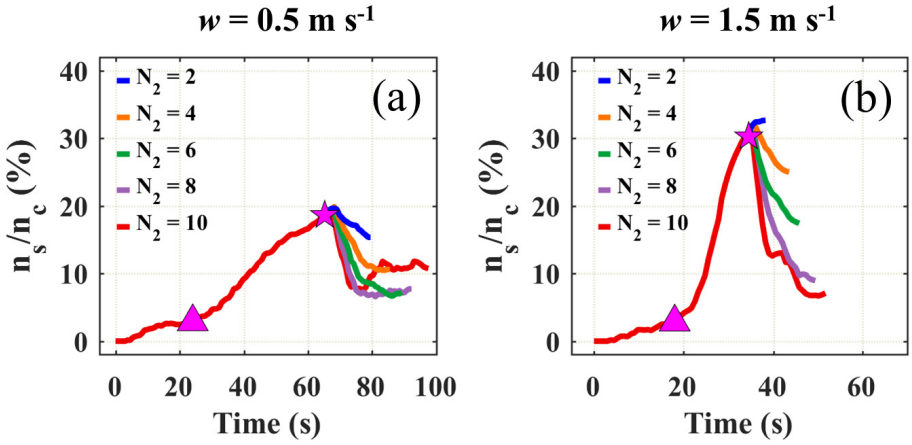

Fig. 4. Temporal evolutions of the ratios of (a, b) small droplet number concentration (n_s) to total droplet number concentration (n_c) for the entrained environmental air blob numbers of the second entrainment-mixing process (N_2) equal to 2, 4, 6, 8, and 10. Left: vertical velocity (w) = 0.5 m s^{-1}. Right: w = 1.5 m s^{-1}. The triangle and pentagram represent the ending of the first entrainment-mixing process and the beginning of the second entrainment-mixing process, respectively.

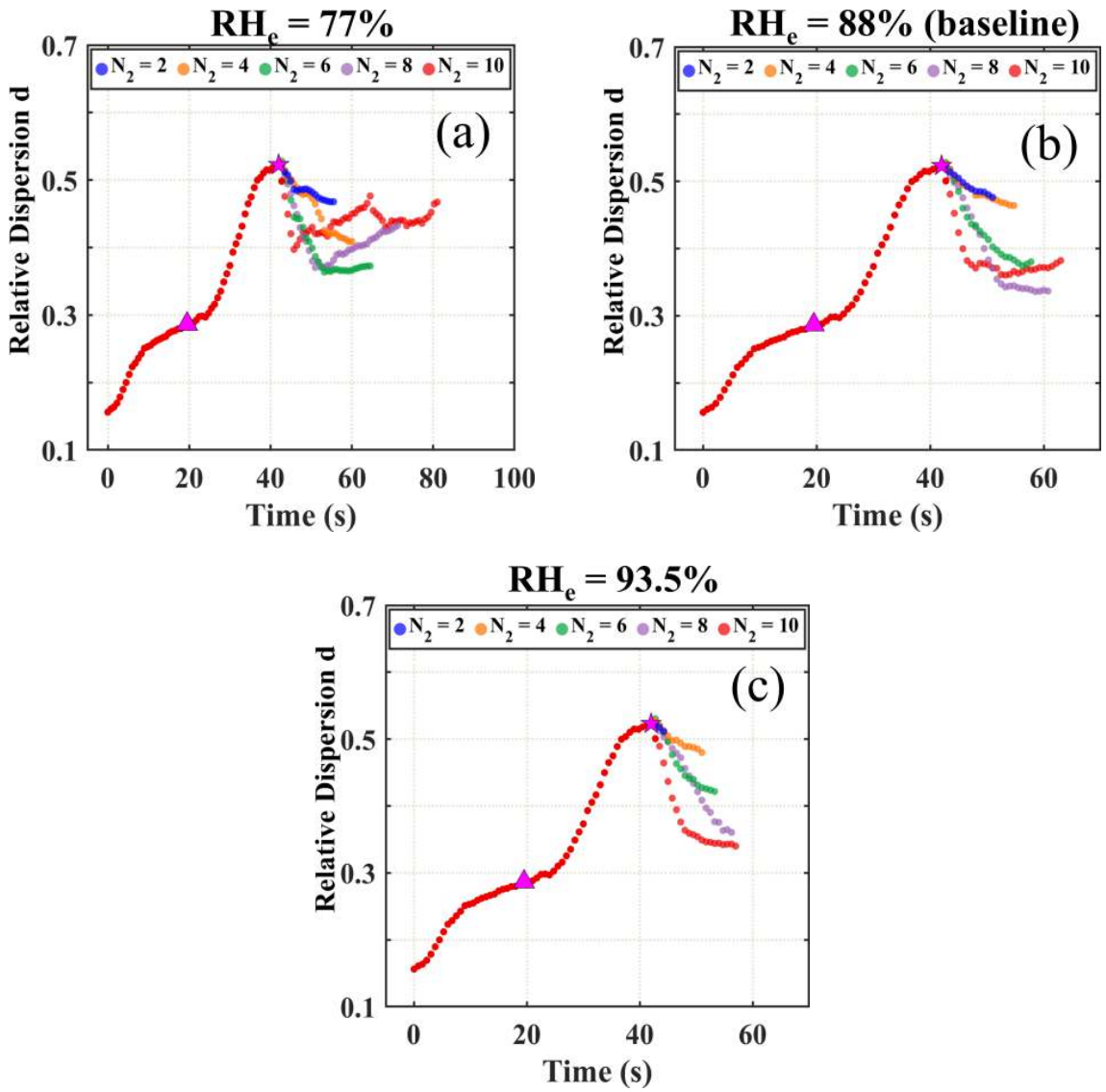

Fig. 5. As in Fig. 3, except for relative humidity of entrained air (RH$_e$).

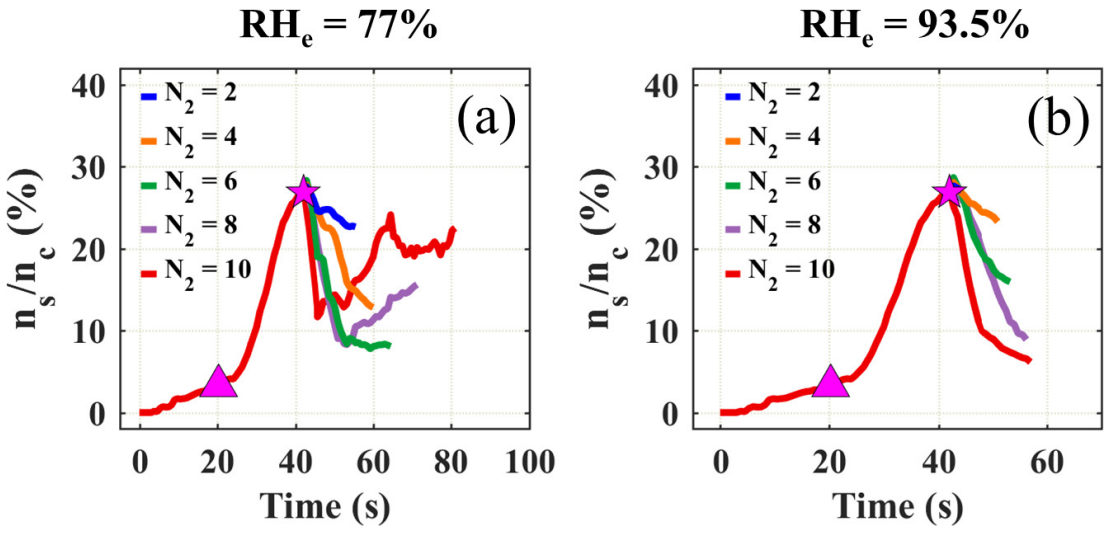

Fig. 6. As in Fig. 4, except for relative humidity of entrained air (RH$_e$).

increases for $N_2 \geq 8$ when $RH_e = 77\%$, due to the evaporation of small droplets and partial evaporation of big droplets, respectively (Fig. 6a). Therefore, d and λ are positively correlated when N_2 increases from 6 to 10. In contrast, when $RH_e = 93.5\%$, n_s/n_c decreases with mixing time (Fig. 6b). The new saturation is easier to achieve by the evaporation dominated by the newly formed small droplets for $N_2 \leq 10$. Overall, the amount of droplet evaporation to restore a new saturation of entrained environmental air decreases as RH_e increases. The evaporation dominated by small droplets is more likely to get the entrained environmental air saturated, resulting in a negative correlation between d and λ.

3.2.3. *Turbulence Dissipation Rate*

Figure 7 shows the temporal evolutions of d when ε increases from 5×10^{-4} to 1×10^{-2} m^2 s^{-3} (Case 4 in Table 1). The relationship between d and λ is negative for $N_2 \leq 8$ and positive for $N_2 \geq 8$ for different ε values. Comparisons of the behaviors of small droplets are made between $\varepsilon = 5 \times 10^{-4}$ and 1×10^{-2} m^2 s^{-3}. Figures. 8a and 8b show that n_s/n_c in the low turbulence intensity case is slightly greater than the strong one (31% vs. 26%). Due to the slight difference in the number of small droplets before the second entrainment-mixing process under the low and high ε conditions, the signs of the relationship between d and λ are not significantly affected by ε. However, it is still found that the positive relationship between d and λ for $N_2 \geq 8$ is stronger for the higher ε condition. Since mixing between cloud and environmental air is stronger for the higher ε condition, big droplets are more likely to contact with the environmental air and experience partial evaporation to increase the number concentration of small droplets (Fig. 8). Therefore, when ε is 5×10^{-4} m^2 s^{-3}, the number concentration of small droplets for $N_2 = 10$ is only a little bit higher than that for $N_2 = 8$. When

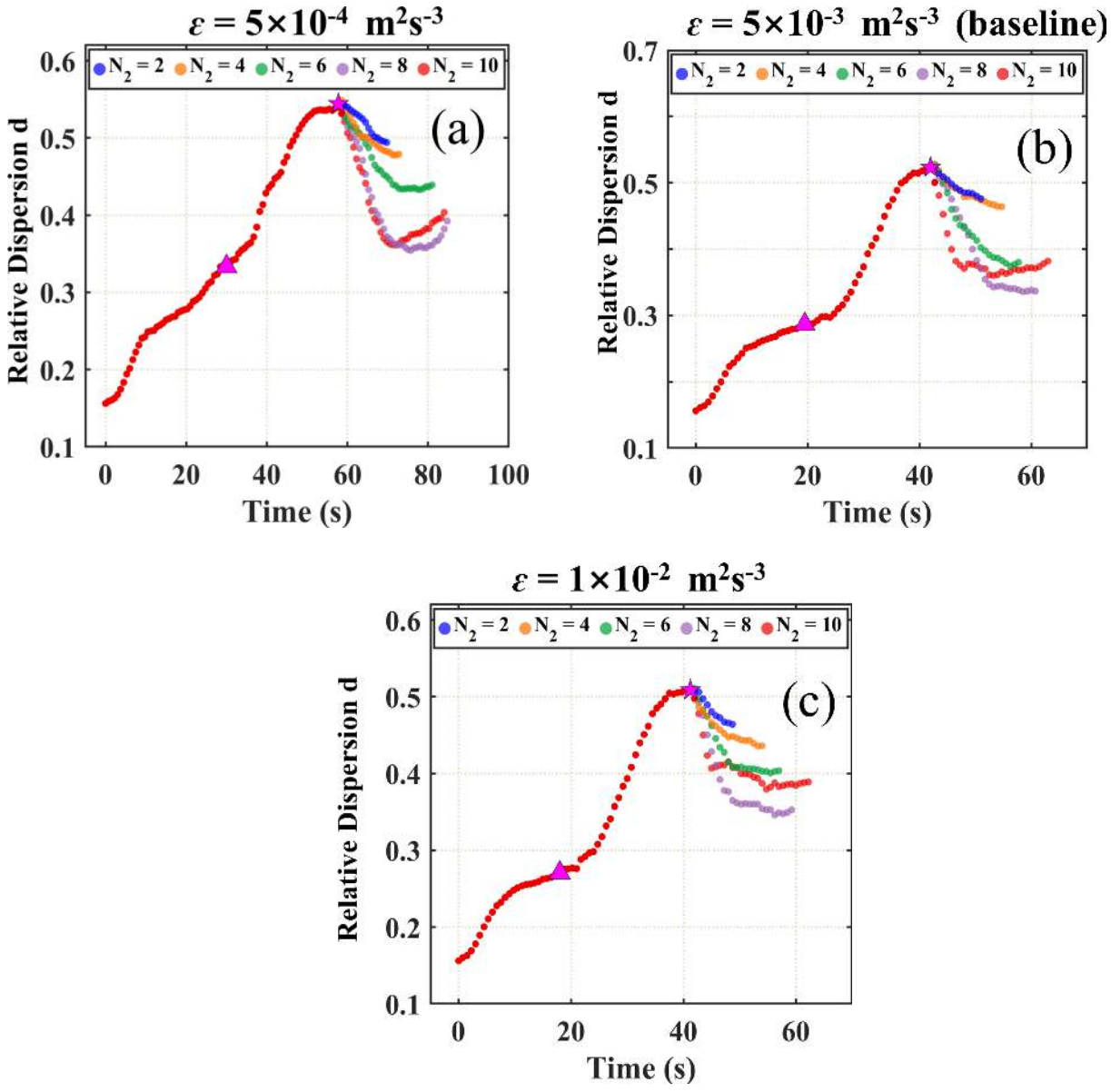

Fig. 7. As in Fig. 3, except for turbulence dissipation rate (ε).

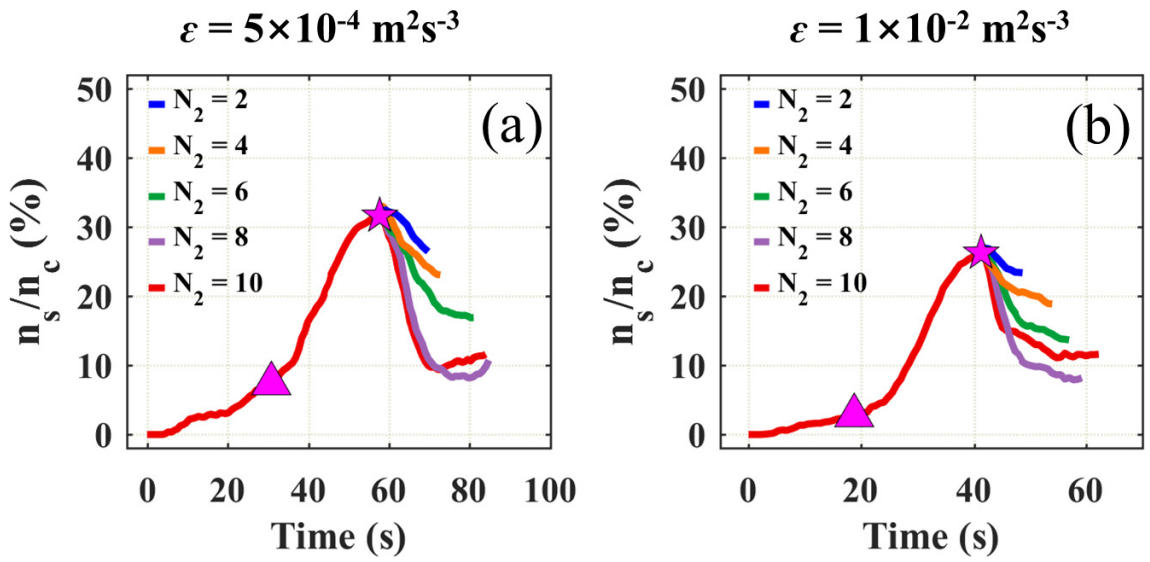

Fig. 8. As in Fig. 4, except for turbulence dissipation rate (ε).

ε is higher (1×10^{-2} m^2 s^{-3}), the number concentration of small droplets for $N_2 = 10$ is much higher than that for $N_2 = 8$.

3.2.4. *Initial Droplet Number Concentration*

In the EMPM, CCN is assumed to be at equilibrium sizes, and water vapor can directly condense on CCN. Such a treatment might affect n_i. To study the effects of n_i uncertainty, sensitivity tests are carried out for n_i = 69.1, 119.4 (baseline case), and 552.6 cm^{-3} (Case 5 in Table 1). Figures 9a and 9b show that d and λ are negatively correlated for $N_2 \leqslant 8$ and positively correlated for $N_2 \geqslant 8$ when n_i = 69.1 and 119.4 cm^{-3}. However, d and λ are positively correlated for $N_2 \leqslant 10$ when n_i = 552.6 cm^{-3} (Fig. 9c). For n_i = 69.1 cm^{-3}, the competition for water vapor between droplets is identified to be weak and is conducive to the growth of entrained CCN into small droplets. As a result, n_s/n_c increases to 39% (Fig. 10a) before the second entrainment-mixing process. The evaporation dominated by these small droplets causes the entrained environmental air to be saturated, except for N_2 = 10. In contrast, high n_i increases the competition for water vapor and reduces supersaturation in the cloud (Abbott and Cronin, 2021). Further, condensation on the entrained CCN is inhibited. Therefore, the value of n_s/n_c before the second entrainment-mixing process is low, accounting for 8%, and n_s/n_c increases with increasing N_2 (Fig. 10b). Therefore, the evaporation of big droplets dominates the second entrainment-mixing process, and d and λ are positively correlated.

3.2.5. *Initial Liquid Water Content*

Figure 11 shows the temporal evolutions of d when LWC$_i$ = 0.25, 0.5 (baseline case), and 0.75 g m^{-3} (Case 6 in Table 1). Here, the variations in LWC$_i$ are realized by altering n_i and maintaining a r_{vi} of 10.0 μm. Based on the results, d and λ are negatively correlated for $N_2 \leqslant 8$ and positively correlated for $N_2 \geqslant 8$ when LWC$_i$ = 0.5 and 0.75 g m^{-3} (Figs. 11b, 11c). In contrast, d and λ are negatively correlated for $N_2 \leqslant 6$ and positively correlated for $N_2 \geqslant 6$ when LWC$_i$ = 0.25 g m^{-3} (Fig. 11a). The value of n_s/n_c significantly increases to 49% when LWC$_i$ = 0.25 g m^{-3} (Fig. 12a). The entrained environmental air for N_2 = 8, 10 cannot be saturated by the evaporation of these small droplets alone. In contrast, n_s/n_c is 13% when LWC$_i$ = 0.75 g m^{-3} (Fig. 12b), and the entrained environmental air for N_2 = 10 cannot be saturated by the evaporation of small droplets alone. Obviously, the lower LWC$_i$ has more small droplets due to the lower competition for water vapor but supports the positive relationship because LWC$_i$ reflects the ability of the cloud to compensate for the supersaturation deficit. When LWC$_i$ is lower, the compensation is weaker. The evaporation of small droplets is not sufficient to saturate entrained environmental air, and thus the evaporation of big droplets becomes more significant, which favors the positive correlation between d and λ.

3.3. *Conceptual Model*

Based on the above detailed analyses of the impacting factors, a conceptual model is established as shown in Fig. 13 to illustrate the formation of the positive and negative correlations between d and λ. Three processes, namely the first entrainment-mixing process, subsequent ascent, and the second entrainment-mixing process are labeled as "Mix 1", "adiabatic", and "Mix 2", respectively. During "Mix 2", the relationship between d and λ is dependent on whether CCN is entrained during "Mix 1". If the entrained environmental air contains CCN, the growth of entrained CCN into small droplets significantly increases d during the "adiabatic" process. During the subsequent "Mix 2", small droplets evaporate significantly. Once the new saturation of environmental air can be achieved dominantly by the evaporation of newly formed small droplets from the entrained CCN, the evaporation of big droplets is weak. The relationship between d and λ is negatively correlated. Otherwise, the evaporation of big droplets would be needed to saturate entrained environmental

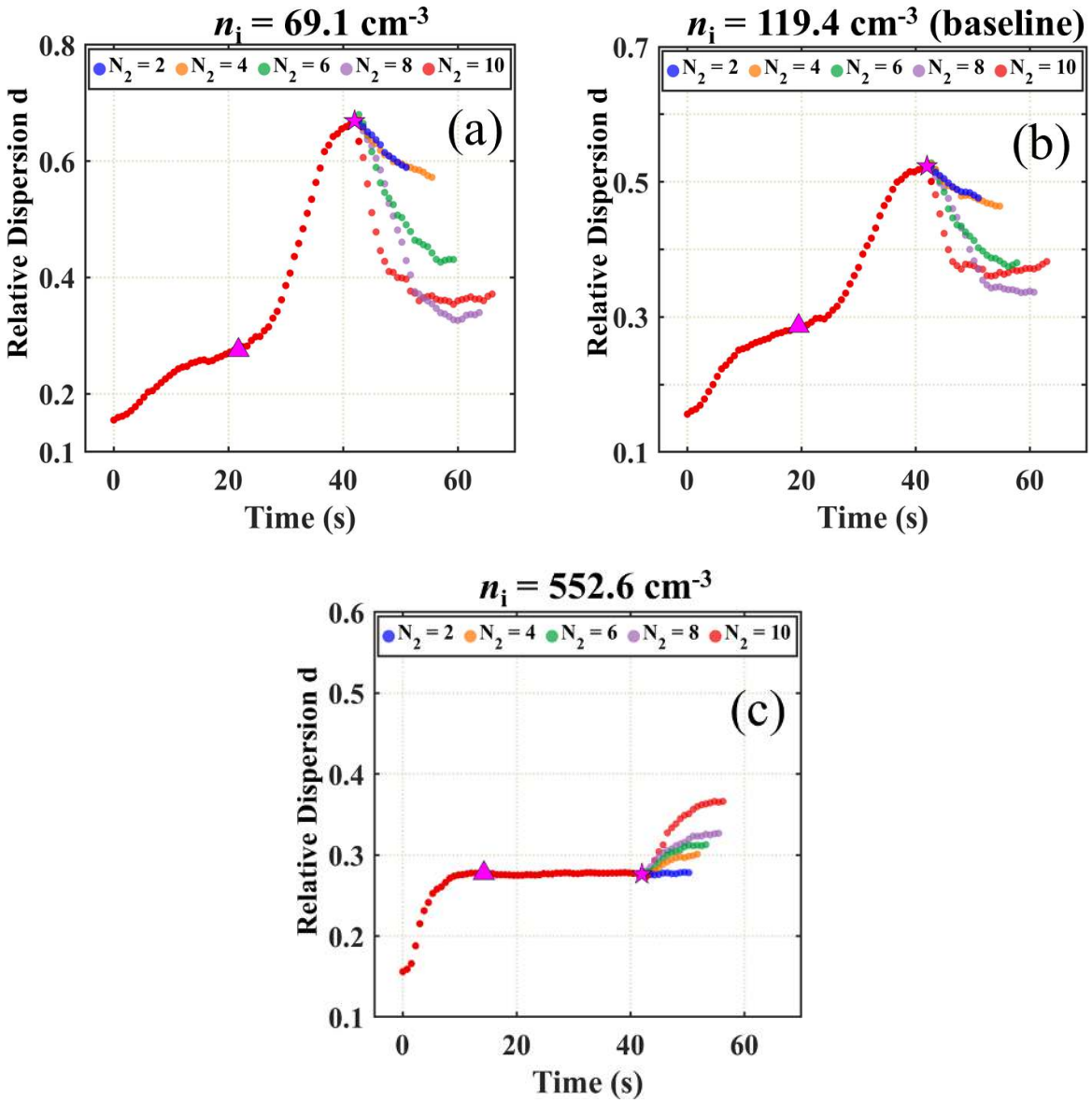

Fig. 9. As in Fig. 3, except for initial droplet number concentration (n_i).

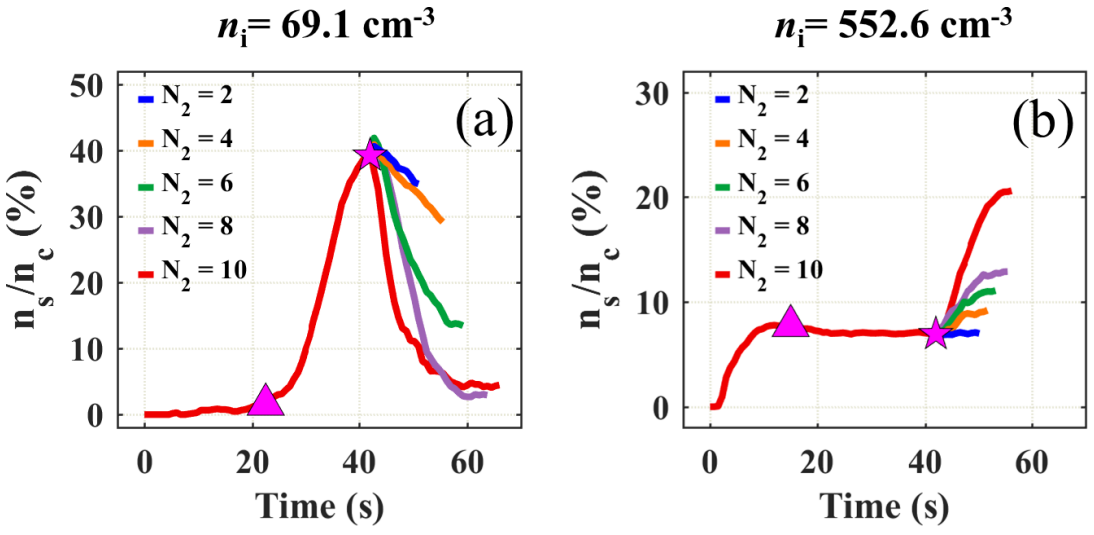

Fig. 10. As in Fig. 4, except for initial droplet number concentration (n_i).

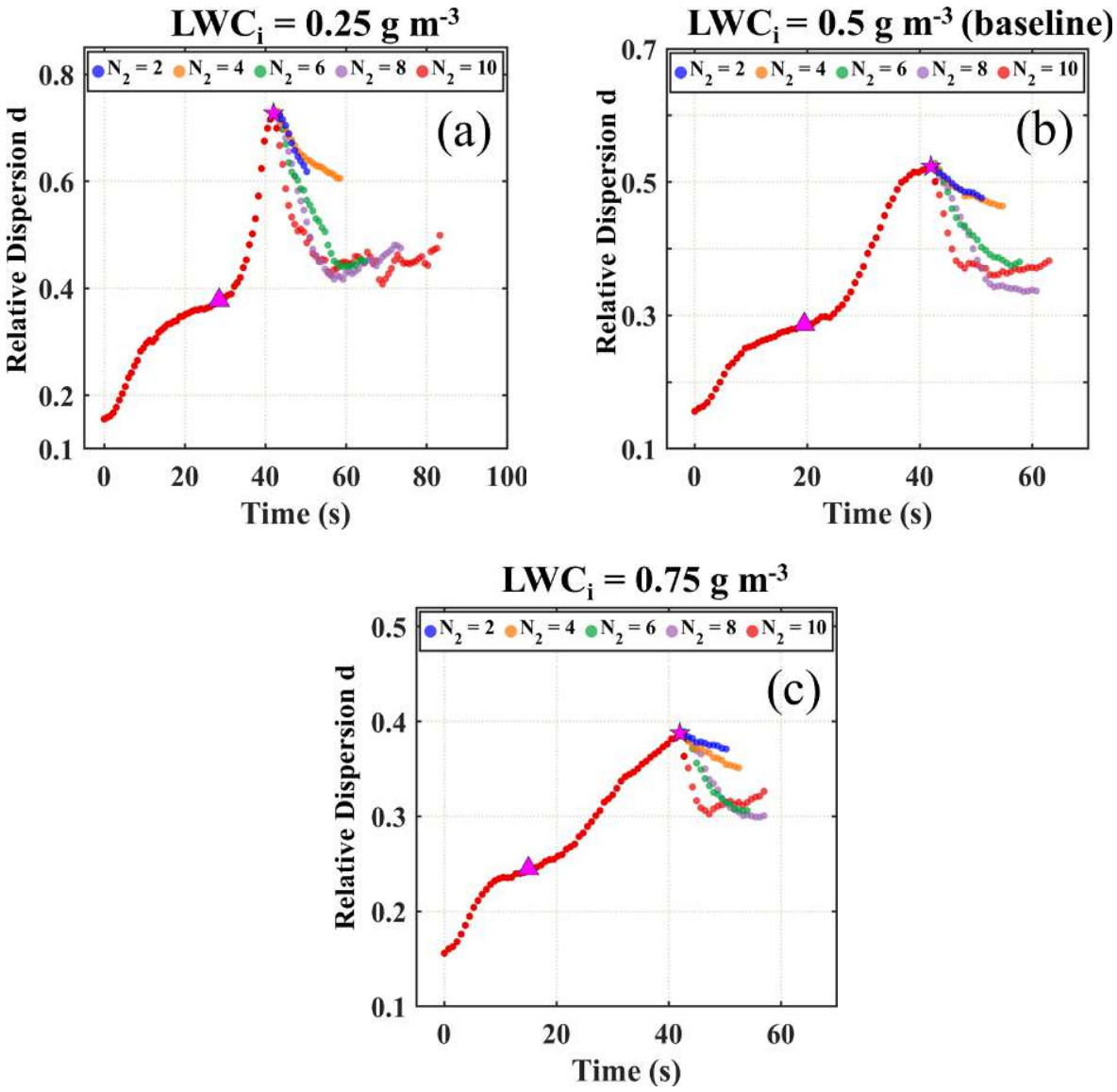

Fig. 11. As in Fig. 3, except for initial liquid water content (LWC$_i$).

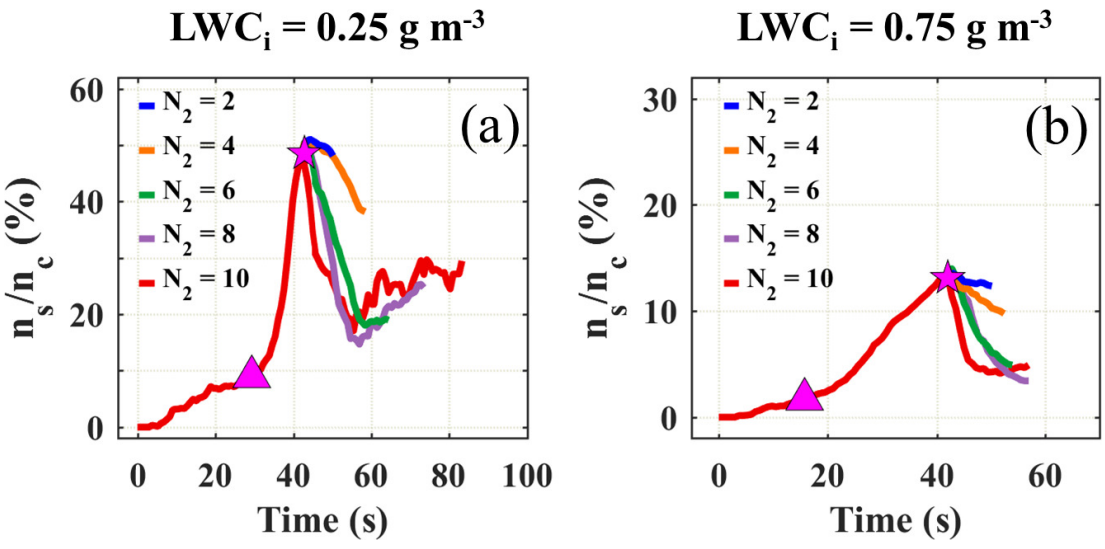

Fig. 12. As in Fig. 4, except for initial liquid water content (LWC$_i$).

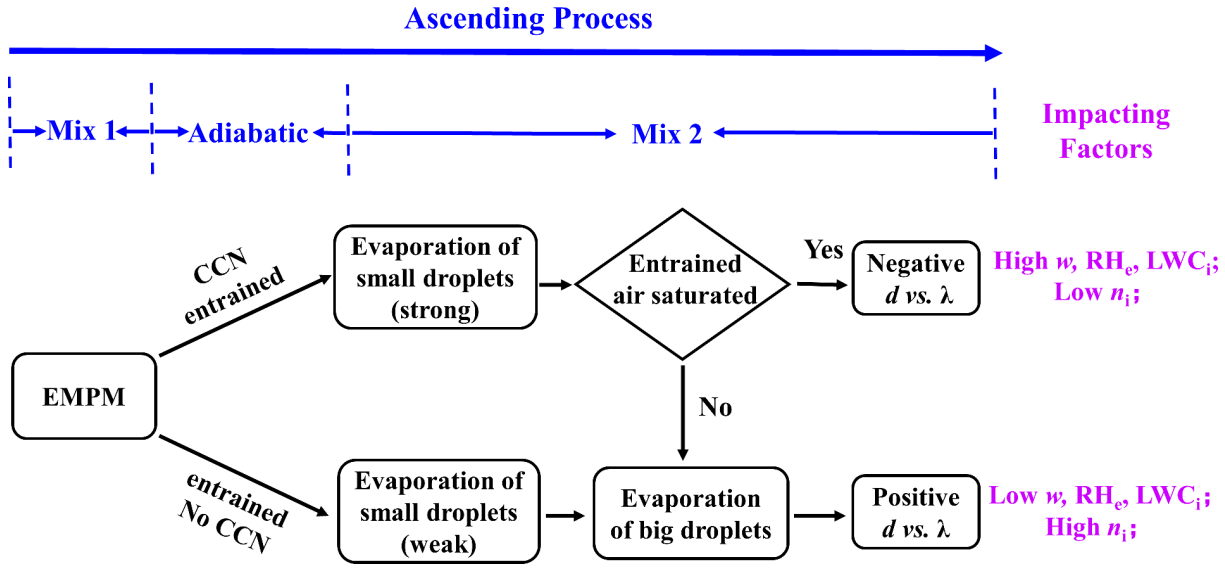

Fig. 13. Flow diagram illustrating the formation of the positive/negative correlation between relative dispersion (d) and entrainment rate (λ). During the ascending process, the first and second entrainment-mixing processes are labeled as "Mix 1" and "Mix 2", as well as "Adiabatic" for the adiabatic ascending process. The impacting factors are: vertical velocity (w), relative humidity of entrained air (RH_e), initial droplet number concentration (n_i), and initial liquid water content (LWC_i).

air, which contributes to the positive correlation between d and λ. High w, RH_e, LWC_i, and low n_i are more likely to cause a negative correlation between d and λ. In contrast, the positive correlation is mainly caused by low w, RH_e, LWC_i, and high n_i. Further, the correlations are not strongly affected by turbulence dissipation rate, though a higher dissipation rate results in a more significant positive correlation for a larger entrainment rate. However, if the entrained environmental air does not contain CCN, the small droplets are too few in number to saturate the entrained environmental air. As a result, the evaporation of big droplets dominates the mixing process, and d and λ are positively correlated.

4. Conclusions

Using the EMPM, this study reproduces the positive/negative correlation between cloud droplet spectral relative dispersion (d) and entrainment rate (λ) found in previous assessments. The mechanisms dominating the relationships and the impacting factors are also investigated herein.

The positive/negative correlation between d and λ is determined by whether the evaporation of small or big droplets dominates the entrainment-mixing process and further saturates the entrained environmental air. If the new saturation can be dominantly achieved by evaporation of small droplets, d and λ are negatively correlated. However, if the evaporation of big droplets is needed to obtain new saturation, d and λ are positively correlated. When entrained environmental air does not contain CCN, d and λ are positively correlated. However, when entrained environmental air contains CCN, condensation on CCN forms many small droplets, which is critical for the negative correlation between d and λ.

The factors affecting small droplet number concentration and the relationship between d and λ, including vertical velocity, relative humidity of entrained air, initial droplet number concentration, initial liquid water content, and turbulence dissipation rate, were determined in this study.

First, high vertical velocity is favorable for the negative correlation between d and λ; this is because stronger updrafts produce higher supersaturation, enabling more entrained CCN to grow into small droplets.

Second, high relative humidity of entrained environmental air is another factor that favors a negative correlation between d and λ. As relative humidity increases, a lower amount of droplet evaporation is needed to restore a new saturation. As a result, small droplets are more likely to dominate the evaporation process to saturate the entrained environmental air, which contributes to the negative correlation between d and λ.

Third, low initial droplet number concentration is favorable for the negative correlation between d and λ. When the initial droplet number concentration is low, the competition for water vapor is weak, which increases supersaturation and promotes the formation of small droplets from the entrained CCN.

Fourth, high initial liquid water content is also favorable for the negative correlation between d and λ. For higher initial liquid water content, new saturation is easier to achieve by the evaporation of small droplets.

Finally, the signs of the relationship between d and λ are not strongly affected by turbulence dissipation rate, but the positive relationship between d and λ for larger entrainment rates is more significant for the higher dissipation rate condition. The above results are further presented as a conceptual model to summarize the factors affecting the relationship between d and λ.

Several points are noteworthy. First, when environmental

air including cloud condensation nuclei (CCN) is entrained, the same-sized segment of the parcel's cloudy air is replaced with the environmental air instantaneously (Krueger, 1993; Krueger et al., 1997, 2008; Su et al., 1998; Krueger and Lehr, 2006; Tölle and Krueger, 2014). This assumption is generally valid because many previous studies indicate that turbulence is both spatially and temporally intermittent (Frisch, 1980; Sreenivasan, 1985; Mahrt, 1989; She et al., 1990; Lohse and Grossmann, 1993). It would be of interest to set the entrainment process to last for a certain length of time and conduct sensitivity tests to the timescale in future studies.

Second, this study reconciles the contrasting relationships between d and λ and reveals the underlying mechanisms. The results will be helpful for improving entrainment-mixing parameterizations (Lu et al., 2013b; Luo et al., 2020; Xu et al., 2022), especially for initial wide cloud droplet size distributions. Previous studies have found that it is challenging to understand entrainment-mixing mechanisms when initial cloud droplet size distributions are wide (Pinsky et al., 2016; Pinsky and Khain, 2018; Luo et al., 2021). Recently, Luo et al. (2021) developed a new method to quantify entrainment-mixing mechanisms for size distributions with different widths and emphasized the importance of small droplets. Similarly, it is found in this study that small droplets related to entrained CCN play important roles in determining the relationship between d and λ. Therefore, it would be interesting to further examine the interactions between entrainment-mixing mechanisms, λ, cloud droplet size distribution, and aerosol.

Third, as climate warms, wind shear will increase (Nolan and Rappin, 2008; Lee et al., 2019), enhancing turbulence intensity. We speculate that the entrainment and mixing processes between cloud and its environment will become more significant. This will affect cloud fraction, cloud depth, cloud microphysics, and further climate sensitivity and aerosol indirect effects.

APPENDIX

Terms Used in Droplet Condensation/Evaporation Equation

The condensation/evaporation of droplets is described by Fukuta and Walter (1970):

$$r_j \frac{\mathrm{d}r_j}{\mathrm{d}t} = \frac{S - A_1 + A_2}{A_3 + A_4} ,$$

$$S = \frac{q_\mathrm{v}}{q_\mathrm{vs}} - 1 ,$$

where r_j is the radius of the jth droplet; A_1 and A_2 are two terms for droplet curvature and solution effects, respectively; A_3 and A_4 are the vapor diffusion and heat conduction terms; S is the supersaturation; q_v is the water vapor mixing ratio and q_vs is the saturated water vapor mixing ratio. Please see Su et al. (1998) for more descriptions of A_1–A_4.

Acknowledgements. The authors thank Sinan GAO and Zhuangzhuang ZHOU in NUIST for helpful discussions. This research is supported by the National Natural Science Foundation of China (Grant Nos. 41822504, 42175099, 42027804, 42075073 and 42075077), and the National Center of Meteorology, Abu Dhabi, UAE under the UAE Research Program for Rain Enhancement Science. LIU is supported by the U.S. Department of Energy Atmospheric System Research (ASR) Program (DE-SC00112704) and Solar Energy Technologies Office (SETO) under Award 33504. LUO is supported by Research Fund of Civil Aviation Flight University of China (J2022-037), LI is supported by Research Fund of Civil Aviation Flight University of China (09005001), and WU is supported by Research on Key of Man-machine Ring in Plateau Flight (FZ2020ZZ03). The simulation data are stored in https://data.mendeley.com/datasets/v38k2hd95b/draft?a=ad380244-94c2-4762-9bc2-ec24a164f234. The numerical calculations in this paper have been performed at the Supercomputing Center of Nanjing University of Information Science and Technology.

Electronic supplementary material: Supplementary material is available in the online version of this article at https://doi.org/10.1007/s00376-022-1419-5.

REFERENCES

Abbott, T. H., and T. W. Cronin, 2021: Aerosol invigoration of atmospheric convection through increases in humidity. *Science*, **371**, 83–85, https://doi.org/10.1126/science.abc5181.

Ackerman, A. S., and Coauthors, 2009: Large-eddy simulations of a drizzling, stratocumulus-topped marine boundary layer. *Mon. Wea. Rev.*, **137**, 1083–1110, https://doi.org/10.1175/2008MWR2582.1.

Axelsen, S. L., 2005: The role of relative humidity on shallow cumulus dynamics; results from a large eddy simulation model. Utrecht, Netherlands: Utrecht University.

Baker, M. B., R. G. Corbin, and J. Latham, 1980: The influence of entrainment on the evolution of cloud droplet spectra: I. A model of inhomogeneous mixing. *Quart. J. Roy. Meteor. Soc.*, **106**, 581–598, https://doi.org/10.1002/qj.49710644914.

Bera, S., 2021: Droplet spectral dispersion by lateral mixing process in continental deep cumulus clouds. *Journal of Atmospheric and Solar-Terrestrial Physics*, **214**, 105550, https://doi.org/10.1016/j.jastp.2021.105550.

Bera, S., T. V. Prabha, and W. W. Grabowski, 2016a: Observations of monsoon convective cloud microphysics over India and role of entrainment-mixing. *J. Geophys. Res.*, **121**, 9767–9788, https://doi.org/10.1002/2016JD025133.

Bera, S., G. Pandithurai, and T. V. Prabha, 2016b: Entrainment and droplet spectral characteristics in convective clouds during transition to monsoon. *Atmospheric Science Letters*, **17**, 286–293, https://doi.org/10.1002/asl.657.

Burnet, F., and J.-L. Brenguier, 2007: Observational study of the entrainment-mixing process in warm convective clouds. *J. Atmos. Sci.*, **64**, 1995–2011, https://doi.org/10.1175/JAS3928.1.

Chandrakar, K. K., W. Cantrell, K. Chang, D. Ciochetto, D. Niedermeier, M. Ovchinnikov, R. A. Shaw, and F. Yang, 2016: Aerosol indirect effect from turbulence-induced broadening

of cloud-droplet size distributions. *Proceedings of the National Academy of Sciences of the United States of America*, **113**, 14 243–14 248, https://doi.org/10.1073/pnas.1612686113.

Chen, J. Y., Y. G. Liu, M. H. Zhang, and Y. R. Peng, 2016: New understanding and quantification of the regime dependence of aerosol-cloud interaction for studying aerosol indirect effects. *Geophys. Res. Lett.*, **43**, 1780–1787, https://doi.org/10.1002/2016GL067683.

Chen, J. Y., Y. G. Liu, and M. H. Zhang, 2020: Effects of lateral entrainment mixing with entrained aerosols on cloud microphysics. *Geophys. Res. Lett.*, **47**, e2020GL087667, https://doi.org/10.1029/2020GL087667.

Cooper, W. A., 1989: Effects of variable droplet growth histories on droplet size distributions. Part I: Theory. *J. Atmos. Sci.*, **46**, 1301–1311, https://doi.org/10.1175/1520-0469(1989)046<1301:EOVDGH>2.0.CO;2.

Cooper, W. A., S. G. Lasher-Trapp, and A. M. Blyth, 2013: The influence of entrainment and mixing on the initial formation of rain in a warm cumulus cloud. *J. Atmos. Sci.*, **70**, 1727–1743, https://doi.org/10.1175/JAS-D-12-0128.1.

de Rooy, W. C., and Coauthors, 2013: Entrainment and detrainment in cumulus convection: An overview. *Quart. J. Roy. Meteor. Soc.*, **139**, 1–19, https://doi.org/10.1002/qj.1959.

Devenish, B. J., and Coauthors, 2012: Droplet growth in warm turbulent clouds. *Quart. J. Roy. Meteor. Soc.*, **138**, 1401–1429, https://doi.org/10.1002/qj.1897.

Frisch, U., 1980: Fully developed turbulence and intermittency. *Annals of the New York Academy of Sciences*, **357**, 359–367, https://doi.org/10.1111/j.1749-6632.1980.tb29703.x.

Fukuta, N., and L. A. Walter, 1970: Kinetics of hydrometeor growth from a vapor-spherical model. *J. Atmos. Sci.*, **27**, 1160–1172, https://doi.org/10.1175/1520-0469(1970)027<1160:KOHGFA>2.0.CO;2.

Gao, S. N., C. S. Lu, Y. G. Liu, F. Mei, J. Wang, L. Zhu, and S. Q. Yan, 2020: Contrasting scale dependence of entrainment-mixing mechanisms in stratocumulus clouds. *Geophys. Res. Lett.*, **47**, e2020GL086970, https://doi.org/10.1029/2020GL086970.

Gao, S., and Coauthors, 2021: Comprehensive quantification of height dependence of entrainment mixing between stratiform cloud top and environment. *Atmospheric Chemistry and Physics*, **21**, 11 225–11 241, https://doi.org/10.5194/acp-21-11225-2021.

Gao, Z., Y. G. Liu, X. L. Li, and C. S. Lu, 2018: Investigation of turbulent entrainment-mixing processes with a new particle-resolved direct numerical simulation model. *J. Geophys. Res.*, **123**, 2194–2214, https://doi.org/10.1002/2017JD027507.

Gerber, H. E., G. M. Frick, J. B. Jensen, and J. G. Hudson, 2008: Entrainment, mixing, and microphysics in trade-wind cumulus. *J. Meteor. Soc. Japan*, **86A**, 87–106, https://doi.org/10.2151/jmsj.86A.87.

Guo, X. H., C. S. Lu, T. L. Zhao, Y. G. Liu, G. J. Zhang, and S. Luo, 2018: Observational study of the relationship between entrainment rate and relative dispersion in deep convective clouds. *Atmospheric Research*, **199**, 186–192, https://doi.org/10.1016/j.atmosres.2017.09.013.

Hoffmann, F., H. Siebert, J. Schumacher, T. Riechelmann, J. Katzwinkel, B. Kumar, P. Götzfried, and S. Raasch, 2014: Entrainment and mixing at the interface of shallow cumulus clouds: Results from a combination of observations and simulations. *Meteor. Z.*, **23**, 349–368, https://doi.org/10.1127/0941-2948/2014/0597.

Hoffmann, F., S. Raasch, and Y. Noh, 2015: Entrainment of aerosols and their activation in a shallow cumulus cloud studied with a coupled LCM–LES approach. *Atmospheric Research*, **156**, 43–57, https://doi.org/10.1016/j.atmosres.2014.12.008.

Houze, R. A. Jr., 1993: *Cloud Dynamics*. Academic Press.

Hsieh, W. C., H. Jonsson, L.-P. Wang, G. Buzorius, R. C. Flagan, J. H. Seinfeld, and A. Nenes, 2009: On the representation of droplet coalescence and autoconversion: Evaluation using ambient cloud droplet size distributions. *J. Geophys. Res.*, **114**, D07201, https://doi.org/10.1029/2008JD010502.

Hudson, J. G., S. Noble, and V. Jha, 2012: Cloud droplet spectral width relationship to CCN spectra and vertical velocity. *J. Geophys. Res.*, **117**, D11211, https://doi.org/10.1029/2012JD017546.

Johnson, D. B., 1993: The onset of effective coalescence growth in convective clouds. *Quart. J. Roy. Meteor. Soc.*, **119**, 925–933, https://doi.org/10.1002/qj.49711951304.

Jonas, P. R., 1990: Observations of cumulus cloud entrainment. *Atmospheric Research*, **25**, 105–127, https://doi.org/10.1016/0169-8095(90)90008-Z.

Kerstein, A. R., 1991: Linear-eddy modelling of turbulent transport. Part 6. Microstructure of diffusive scalar mixing fields. *J. Fluid Mech.*, **231**, 361–394, https://doi.org/10.1017/S0022112091003439.

Kerstein, A. R., 1992: Linear eddy modeling of turbulent transport. Part 7 Finite rate chemistry and multi-stream mixing. *J. Fluid Mech.*, **240**, 289–313, https://doi.org/10.1017/S0022112092000107.

Khain, A., M. Pinsky, and L. Magaritz-Ronen, 2018: Physical interpretation of mixing diagrams. *J. Geophys. Res.*, **123**, 529–542, https://doi.org/10.1002/2017JD027124.

Krueger, S. K., 1993: Linear eddy modeling of entrainment and mixing in stratus clouds. *J. Atmos. Sci.*, **50**, 3078–3090, https://doi.org/10.1175/1520-0469(1993)050<3078:LEMOEA>2.0.CO;2.

Krueger, S. K., P. Lehr, and C. Su, 2006: How entrainment and mixing scenarios affect droplet spectra in cumulus clouds. Preprints, *12th Conference on Cloud Physics*.

Krueger, S. K., C.-W. Su, and P. A. McMurtry, 1997: Modeling entrainment and finescale mixing in cumulus clouds. *J. Atmos. Sci.*, **54**, 2697–2712, https://doi.org/10.1175/1520-0469(1997)054<2697:MEAFMI>2.0.CO;2.

Krueger, S. K., H. Schlueter, and P. Lehr, 2008: Fine-scale modeling of entrainment and mixing of cloudy and clear air. Preprints, *15th International Conference on Clouds and Precipitation, Cancun, Mexico*.

Kumar, B., F. Janetzko, J. Schumacher, and R. A. Shaw, 2012: Extreme responses of a coupled scalar-particle system during turbulent mixing. *New Journal of Physics*, **14**, 115020, https://doi.org/10.1088/1367-2630/14/11/115020.

Kumar, B., J. Schumacher, and R. A. Shaw, 2014: Lagrangian mixing dynamics at the cloudy–clear air interface. *J. Atmos. Sci.*, **71**, 2564–2580, https://doi.org/10.1175/JAS-D-13-0294.1.

Kumar, B., S. Bera, T. V. Prabha, and W. W. Grabowski, 2017: Cloud-edge mixing: Direct numerical simulation and observations in Indian Monsoon clouds. *Journal of Advances in Modeling Earth Systems*, **9**, 332–353, https://doi.org/10.1002/2016MS000731.

Lasher-Trapp, S. G., W. A. Cooper, and A. M. Blyth, 2005: Broad-

ening of droplet size distributions from entrainment and mixing in a cumulus cloud. *Quart. J. Roy. Meteor. Soc.*, **131**, 195–220, https://doi.org/10.1256/qj.03.199.

Lee, S. H., P. D. Williams, and T. H. A. Frame, 2019: Increased shear in the North Atlantic upper-level jet stream over the past four decades. *Nature*, **572**, 639–642, https://doi.org/10.1038/s41586-019-1465-z.

Lehmann, K., H. Siebert, and R. A. Shaw, 2009: Homogeneous and inhomogeneous mixing in cumulus clouds: Dependence on local turbulence structure. *J. Atmos. Sci.*, **66**, 3641–3659, https://doi.org/10.1175/2009JAS3012.1.

Li, Y. Y., and M. H. Zhang, 2017: The role of shallow convection over the Tibetan Plateau. *J. Climate*, **30**, 5791–5803, https://doi.org/10.1175/JCLI-D-16-0599.1.

Liu, Y., P. H. Daum, S. K. Chai, and F. Liu, 2002: Cloud parameterizations, cloud physics, and their connections: An overview. BNL-68995, 26 pp.

Liu, Y. G., 2019: Introduction to the special section on fast physics in climate models: Parameterization, evaluation, and observation. *J. Geophys. Res.*, **124**, 8631–8644, https://doi.org/10.1029/2019JD030422.

Liu, Y. G., and P. H. Daum, 2002: Indirect warming effect from dispersion forcing. *Nature*, **419**, 580–581, https://doi.org/10.1038/419580a.

Liu, Y. G., P. H. Daum, and S. S. Yum, 2006: Analytical expression for the relative dispersion of the cloud droplet size distribution. *Geophys. Res. Lett.*, **33**, L02810, https://doi.org/10.1029/2005GL024052.

Lohse, D., and S. Grossmann, 1993: Intermittency in turbulence. *Physica A: Statistical Mechanics and its Applications*, **194**, 519–531, https://doi.org/10.1016/0378-4371(93)90382-E.

Lu, C., and Coauthors, 2018c: Observational relationship between entrainment rate and environmental relative humidity and implications for convection parameterization. *Geophys. Res. Lett.*, **45**, 13 495–13 504, https://doi.org/10.1029/2018GL080264.

Lu, C. S., Y. G. Liu, S. S. Yum, S. J. Niu, and S. Endo, 2012: A new approach for estimating entrainment rate in cumulus clouds. *Geophys. Res. Lett.*, **39**, L04802, https://doi.org/10.1029/2011GL050546.

Lu, C. S., S. J. Niu, Y. G. Liu, and A. M. Vogelmann, 2013a: Empirical relationship between entrainment rate and microphysics in cumulus clouds. *Geophys. Res. Lett.*, **40**, 2333–2338, https://doi.org/10.1002/grl.50445.

Lu, C. S., Y. G. Liu, S. J. Niu, S. Krueger, and T. Wagner, 2013b: Exploring parameterization for turbulent entrainment-mixing processes in clouds. *J. Geophys. Res.*, **118**, 185–194, https://doi.org/10.1029/2012JD018464.

Lu, C.-S., Y.-G. Liu, S.-J. Niu, and Y.-Q. Xue, 2018a: Broadening of cloud droplet size distributions and warm rain initiation associated with turbulence: An overview. *Atmospheric and Oceanic Science Letters*, **11**, 123–135, https://doi.org/10.1080/16742834.2018.1410057.

Lu, C. S., Y. G. Liu, B. Zhu, S. S. Yum, S. K. Krueger, Y. J. Qiu, S. J. Niu, and S. Luo, 2018b: On which microphysical time scales to use in studies of entrainment-mixing mechanisms in clouds. *J. Geophys. Res.*, **123**, 3740–3756, https://doi.org/10.1002/2017JD027985.

Lu, C. S., and Coauthors, 2020: Reconciling contrasting relationships between relative dispersion and volume-mean radius of cloud droplet size distributions. *J. Geophys. Res.*, **125**, e2019JD031868, https://doi.org/10.1029/2019JD031868.

Luo, S., and Coauthors, 2020: Parameterizations of entrainment-mixing mechanisms and their effects on cloud droplet spectral width based on numerical simulations. *J. Geophys. Res.*, **125**, e2020JD032972, https://doi.org/10.1029/2020JD032972.

Luo, S., C. S. Lu, Y. G. Liu, W. H. Gao, L. Zhu, X. Q. Xu, J. J. Li, and X. H. Guo, 2021: Consideration of initial cloud droplet size distribution shapes in quantifying different entrainment-mixing mechanisms. *J. Geophys. Res.*, **126**, e2020JD034455, https://doi.org/10.1029/2020JD034455.

Ma, J. Z., Y. Chen, W. Wang, P. Yang, H. J. Liu, S. Y. Yang, Z. J. Hu, and J. Lelieveld, 2010: Strong air pollution causes widespread haze-clouds over China. *J. Geophys. Res.*, **115**, D18204, https://doi.org/10.1029/2009JD013065.

Mahrt, L., 1989: Intermittency of atmospheric turbulence. *J. Atmos. Sci.*, **46**, 79–95, https://doi.org/10.1175/1520-0469(1989)046<0079:IOAT>2.0.CO;2.

McFarquhar, G. M., T.-L. Hsieh, M. Freer, J. Mascio, and B. F. Jewett, 2015: The characterization of ice hydrometeor gamma size distributions as volumes in N_0–λ–μ phase space: Implications for microphysical process modeling. *J. Atmos. Sci.*, **72**, 892–909, https://doi.org/10.1175/JAS-D-14-0011.1.

Nolan, D. S., and E. D. Rappin, 2008: Increased sensitivity of tropical cyclogenesis to wind shear in higher SST environments. *Geophys. Res. Lett.*, **35**, L14805, https://doi.org/10.1029/2008GL034147.

Pandithurai, G., S. Dipu, T. V. Prabha, R. S. Maheskumar, J. R. Kulkarni, and B. N. Goswami, 2012: Aerosol effect on droplet spectral dispersion in warm continental cumuli. *J. Geophys. Res.*, **117**, D16202, https://doi.org/10.1029/2011JD016532.

Peng, Y. R., U. Lohmann, R. Leaitch, and M. Kulmala, 2007: An investigation into the aerosol dispersion effect through the activation process in marine stratus clouds. *J. Geophys. Res.*, **112**, D11117, https://doi.org/10.1029/2006JD007401.

Pinsky, M., and A. Khain, 2018: Theoretical analysis of mixing in liquid clouds-Part IV: DSD evolution and mixing diagrams. *Atmospheric Chemistry and Physics*, **18**, 3659–3676, https://doi.org/10.5194/acp-18-3659-2018.

Pinsky, M., A. Khain, A. Korolev, and L. Magaritz-Ronen, 2016: Theoretical investigation of mixing in warm clouds–Part 2: Homogeneous mixing. *Atmospheric Chemistry and Physics*, **16**, 9255–9272, https://doi.org/10.5194/acp-16-9255-2016.

Prabha, T. V., and Coauthors, 2012: Spectral width of premonsoon and monsoon clouds over Indo-Gangetic valley. *J. Geophys. Res.*, **117**, D20205, https://doi.org/10.1029/2011JD016837.

Prabhakaran, P., A. S. M. Shawon, G. Kinney, S. Thomas, W. Cantrell, and R. A. Shaw, 2020: The role of turbulent fluctuations in aerosol activation and cloud formation. *Proceedings of the National Academy of Sciences of the United States of America*, **117**, 16 831–16 838, https://doi.org/10.1073/pnas.2006426117.

Raga, G. B., J. B. Jensen, and M. B. Baker, 1990: Characteristics of cumulus band clouds off the coast of hawaii. *J. Atmos. Sci.*, **47**, 338–356, https://doi.org/10.1175/1520-0469(1990)047<0338:COCBCO>2.0.CO;2.

Randall, D. A., and Coauthors, 2018: 100 years of earth system model development. *Meteor. Monogr.*, **59**, 12.1–12.66, https://doi.org/10.1175/AMSMONOGRAPHS-D-18-0018.1.

Rotstayn, L. D., and Y. G. Liu, 2009: Cloud droplet spectral dispersion and the indirect aerosol effect: Comparison of two treatments in a GCM. *Geophys. Res. Lett.*, **36**, L10801, https://doi.org/10.1029/2009GL038216.

She, Z.-S., E. Jackson, and S. A. Orszag, 1990: Intermittent vortex structures in homogeneous isotropic turbulence. *Nature*, **344**, 226–228, https://doi.org/10.1038/344226a0.

Siebert, H., K. Lehmann, and M. Wendisch, 2006a: Observations of small-scale turbulence and energy dissipation rates in the cloudy boundary layer. *J. Atmos. Sci.*, **63**, 1451–1466, https://doi.org/10.1175/JAS3687.1.

Siebert, H., H. Franke, K. Lehmann, R. Maser, E. W. Saw, D. Schell, R. A. Shaw, and M. Wendisch, 2006b: Probing finescale dynamics and microphysics of clouds with helicopter-borne measurements. *Bull. Amer. Meteor. Soc.*, **87**, 1727–1738, https://doi.org/10.1175/BAMS-87-12-1727.

Slawinska, J., W. W. Grabowski, H. Pawlowska, and H. Morrison, 2012: Droplet activation and mixing in large-eddy simulation of a shallow cumulus field. *J. Atmos. Sci.*, **69**, 444–462, https://doi.org/10.1175/JAS-D-11-054.1.

Small, J. D., and P. Y. Chuang, 2008: New observations of precipitation initiation in warm cumulus clouds. *J. Atmos. Sci.*, **65**, 2972–2982, https://doi.org/10.1175/2008JAS2600.1.

Small, J. D., P. Y. Chuang, and H. H. Jonsson, 2013: Microphysical imprint of entrainment in warm cumulus. *Tellus B: Chemical and Physical Meteorology*, **65**, 19922, https://doi.org/10.3402/tellusb.v65i0.19922.

Sreenivasan, K., 1985: On the fine-scale intermittency of turbulence. *J. Fluid Mech.*, **151**, 81–103, https://doi.org/10.1017/S0022112085000878.

Stanfield, R. E., and Coauthors, 2019: Convective entrainment rates estimated from Aura CO and CloudSat/CALIPSO observations and comparison with GEOS - 5. *J. Geophys. Res.*, **124**, 9796–9807, https://doi.org/10.1029/2019JD030846.

Su, C.-W., S. K. Krueger, P. A. McMurtry, and P. H. Austin, 1998: Linear eddy modeling of droplet spectral evolution during entrainment and mixing in cumulus clouds. *Atmospheric Research*, **47–48**, 41–58, https://doi.org/10.1016/S0169-8095(98)00039-8.

Tas, E., I. Koren, and O. Altaratz, 2012: On the sensitivity of droplet size relative dispersion to warm cumulus cloud evolution. *Geophys. Res. Lett.*, **39**, L13807, https://doi.org/10.1029/2012GL052157.

Tas, E., A. Teller, O. Altaratz, D. Axisa, R. Bruintjes, Z. Levin, and I. Koren, 2015: The relative dispersion of cloud droplets: Its robustness with respect to key cloud properties. *Atmospheric Chemistry and Physics*, **15**, 2009–2017, https://doi.org/10.5194/acp-15-2009-2015.

Telford, J. W., and S. K. Chai, 1980: A new aspect of condensation theory. *Pure and Applied Geophysics*, **118**, 720–742, https://doi.org/10.1007/BF01593025.

Tölle, M. H., and S. K. Krueger, 2014: Effects of entrainment and mixing on droplet size distributions in warm cumulus clouds. *Journal of Advances in Modeling Earth Systems*, **6**, 281–299, https://doi.org/10.1002/2012MS000209.

Turner, J. S., 1962: The 'starting plume' in neutral surroundings. *J. Fluid Mech.*, **13**, 356–368, https://doi.org/10.1017/S0022112062000762.

Wallace, J. M., and P. V. Hobbs, 2006: *Atmospheric Science*: *An Introductory Survey*. 2nd ed. Elsevier.

Wang, M. Q., Y. R. Peng, Y. G. Liu, Y. Liu, X. N. Xie, and Z. Y. Guo, 2020a: Understanding cloud droplet spectral dispersion effect using empirical and semi-analytical parameterizations in NCAR CAM5.3. *Earth and Space Science*, **7**, e2020EA001276, https://doi.org/10.1029/2020EA001276.

Wang, Y., and Coauthors, 2019: A new method for distinguishing unactivated particles in cloud condensation nuclei measurements: Implications for aerosol indirect effect evaluation. *Geophys. Res. Lett.*, **46**, 14 185–14 194, https://doi.org/10.1029/2019GL085379.

Wang, Y., and Coauthors, 2020b: Microphysical properties of generating cells over the Southern Ocean: Results from SOCRATES. *J. Geophys. Res.*, **125**, e2019JD032237, https://doi.org/10.1029/2019JD032237.

Wang, Y., H. Su, J. H. Jiang, F. Xu, and Y. L. Yung, 2020c: Impact of cloud ice particle size uncertainty in a climate model and implications for future satellite missions. *J. Geophys. Res.*, **125**, e2019JD032119, https://doi.org/10.1029/2019JD032119.

Wang, Y., C. F. Zhao, G. M. McFarquhar, W. Wu, M. Reeves, and J. M. Li, 2021a: Dispersion of droplet size distributions in supercooled non-precipitating stratocumulus from aircraft observations obtained during the Southern Ocean cloud radiation aerosol transport experimental study. *J. Geophys. Res.*, **126**, e2020JD033720, https://doi.org/10.1029/2020JD033720.

Wang, Y., S. J. Niu, C. S. Lu, S. X. Fan, J. J. Lv, X. Q. Xu, Y. C. Jin, and W. Sun, 2021b: A new CCN activation parameterization and its potential influences on aerosol indirect effects. *Atmospheric Research*, **253**, 105491, https://doi.org/10.1016/j.atmosres.2021.105491.

Xie, X. N., X. D. Liu, Y. R. Peng, Y. Wang, Z. G. Yue, and X. Z. Li, 2013: Numerical simulation of clouds and precipitation depending on different relationships between aerosol and cloud droplet spectral dispersion. *Tellus B: Chemical and Physical Meteorology*, **65**, 19054, https://doi.org/10.3402/tellusb.v65i0.19054.

Xu, X. Q., C. S. Lu, Y. G. Liu, W. H. Gao, Y. Wang, Y. M. Cheng, S. Luo, and K. Van Weverberg, 2020: Effects of cloud liquid-phase microphysical processes in mixed-phase cumuli over the Tibetan Plateau. *J. Geophys. Res.*, **125**, e2020JD033371, https://doi.org/10.1029/2020JD033371.

Xu, X. Q., C. Sun, C. S. Lu, Y. G. Liu, G. J. Zhang, and Q. Chen, 2021: Factors affecting entrainment rate in deep convective clouds and parameterizations. *J. Geophys. Res.*, **126**, e2021JD034881, https://doi.org/10.1029/2021JD034881.

Xu, X., and Coauthors, 2022: Influences of an entrainment–mixing parameterization on numerical simulations of cumulus and stratocumulus clouds. *Atmos. Chem. Phys.*, **22**, 5459–5475, https://doi.org/10.5194/acp-22-5459-2022.

Xue, H. W., and G. Feingold, 2006: Large-eddy simulations of trade wind cumuli: Investigation of aerosol indirect effects. *J. Atmos. Sci.*, **63**, 1605–1622, https://doi.org/10.1175/JAS3706.1.

Yang, F., P. Kollias, R. A. Shaw, and A. M. Vogelmann, 2018: Cloud droplet size distribution broadening during diffusional growth: Ripening amplified by deactivation and reactivation. *Atmospheric Chemistry and Physics*, **18**, 7313–7328, https://doi.org/10.5194/acp-18-7313-2018.

Yeom, J. M., S. S. Yum, F. Mei, B. Schmid, J. Comstock, L. A. T. Machado, and M. A. Cecchini, 2019: Impact of secondary droplet activation on the contrasting cloud microphysical relationships during the wet and dry seasons in the Amazon. *Atmospheric Research*, **230**, 104648, https://doi.org/10.1016/j.atmosres.2019.104648.

Yum, S. S., and J. G. Hudson, 2005: Adiabatic predictions and observations of cloud droplet spectral broadness. *Atmospheric Research*, **73**, 203–223, https://doi.org/10.1016/j.atmosres.

2004.10.006.

Yum, S. S., J. Wang, Y. G. Liu, G. Senum, S. Springston, R. McGraw, and J. M. Yeom, 2015: Cloud microphysical relationships and their implication on entrainment and mixing mechanism for the stratocumulus clouds measured during the VOCALS project. *J. Geophys. Res.*, **120**, 5047–5069, https://doi.org/10.1002/2014JD022802.

Zelinka, M. D., D. A. Randall, M. J. Webb, and S. A. Klein, 2017: Clearing clouds of uncertainty. *Nature Climate Change*, **7**, 674–678, https://doi.org/10.1038/nclimate3402.

Zhang, G. J., X. Q. Wu, X. P. Zeng, and T. Mitovski, 2016: Estimation of convective entrainment properties from a cloud-resolving model simulation during TWP-ICE. *Climate Dyn.*, **47**, 2177–2192, https://doi.org/10.1007/s00382-015-2957-7.

Zhao, C. F., Y. M. Qiu, X. B. Dong, Z. E. Wang, Y. R. Peng, B. D. Li, Z. H. Wu, and Y. Wang, 2018: Negative aerosol-cloud r_e relationship from aircraft observations over Hebei, China. *Earth and Space Science*, **5**, 19–29, https://doi.org/10.1002/2017EA000346.

Zhao, C. S., and Coauthors, 2006: Aircraft measurements of cloud droplet spectral dispersion and implications for indirect aerosol radiative forcing. *Geophys. Res. Lett.*, **33**, L16809, https://doi.org/10.1029/2006GL026653.

Zheng, Y. T., Y. N. Zhu, D. Rosenfeld, and Z. Q. Li, 2021: Climatology of cloud-top radiative cooling in marine shallow clouds. *Geophys. Res. Lett.*, **48**, e2021GL094676, https://doi.org/10.1029/2021GL094676.

Zhu, L., and Coauthors, 2021: A new approach for simultaneous estimation of entrainment and detrainment rates in non-precipitating shallow cumulus. *Geophys. Res. Lett.*, **48**, e2021GL093817, https://doi.org/10.1029/2021GL093817.